nature biomedical engineering

Article

https://doi.org/10.1038/s41551-023-01033-1

A one-pot isothermal Cas12-based assay for the sensitive detection of microRNAs

Received: 17 May 2022

Accepted: 29 March 2023

Published online: 27 April 2023

Check for updates

He Yan[1], Yunjie Wen[1], Zimu Tian[1], Nathan Hart[1], Song Han[2], Steven J. Hughes[2] & Yong Zeng[1,3,4]

The use of microRNAs as clinical cancer biomarkers is hindered by the absence of accurate, fast and inexpensive assays for their detection in biofluids. Here we report a one-step and one-pot isothermal assay that leverages rolling-circle amplification and the endonuclease Cas12a for the accurate detection of specific miRNAs. The assay exploits the *cis*-cleavage activity of Cas12a to enable exponential rolling-circle amplification of target sequences and its *trans*-cleavage activity for their detection and for signal amplification. In plasma from patients with pancreatic ductal adenocarcinoma, the assay detected the miRNAs miR-21, miR-196a, miR-451a and miR-1246 in extracellular vesicles at single-digit femtomolar concentrations with single-nucleotide specificity. The assay is rapid (sample-to-answer times ranged from 20 min to 3 h), does not require specialized instrumentation and is compatible with a smartphone-based fluorescence detection and with the lateral-flow format for visual readouts. Simple assays for the detection of miRNAs in blood may aid the development of miRNAs as biomarkers for the diagnosis and prognosis of cancers.

MicroRNAs are endogenous and short non-coding single-stranded RNAs (18–23 nucleotides) that are involved in the post-transcriptional repression of messenger RNAs. Because they participate in various biological processes such as cell proliferation, differentiation and cell death, dysregulated miRNAs are closely linked to the pathogenesis of diseases such as cancers[1–4]. miRNAs were originally studied in tissues, but they have also been discovered in the blood, urine and other body fluids, and found to be associated with ribonucleoprotein complexes or argonaute-2, or encapsulated in exosomes[5]. Probing for circulating miRNAs is therefore a promising strategy in liquid-biopsy-based cancer diagnosis, prognosis and monitoring[2,5,6]. Yet, despite the promise, moving from proof of concept to clinical practice remains a work in progress. One roadblock is the challenge in the high-performance detection of miRNAs in biospecimens due to their short length, high sequence similarity within miRNA families, enormous concentration range in different cell types and biofluids, and the variety of associated origins and carriers[6–9]. Therefore, there is a pressing need of ultrasensitive, specific and robust bioassays and sensors that can facilitate the development of clinically viable miRNA biomarkers of diseases.

Reverse transcription-quantitative polymerase chain reaction (RT-qPCR) has been the gold standard tool for miRNA detection. Distinct from long RNA species, such as mRNAs, short miRNAs necessitate a special RT process to incorporate extended sequences that facilitate PCR amplification and detection[10,11]. Stem-loop and polyadenylation RT assays are two commonly used approaches broadly adapted in many commercial miRNA RT-qPCR kits[8,10]. Alternatively to thermal cycling-based qPCR, which requires sophisticated analytical procedures and instruments, many isothermal assays have been developed to advance miRNA detection[12], including rolling-circle amplification (RCA)[13–15], exponential amplification reaction (EXPAR)[16,17], loop-mediated isothermal amplification (LAMP)[18], hybridization chain reaction[19,20] and catalytic hairpin assembly[21,22]. Despite merits in simplicity and even instrument-free operation, these assays have drawbacks that limit widespread clinical application, such as the non-specific amplification and the high background signal of EXPAR

[1]Department of Chemistry, University of Florida, Gainesville, FL, USA. [2]Department of Surgery, University of Florida College of Medicine, Gainesville, FL, USA. [3]J. Crayton Pruitt Family Department of Biomedical Engineering, University of Florida, Gainesville, FL, USA. [4]University of Florida Health Cancer Center, Gainesville, FL, USA. e-mail: zengy@ufl.edu

https://doi.org/10.1038/s41551-023-01033-1

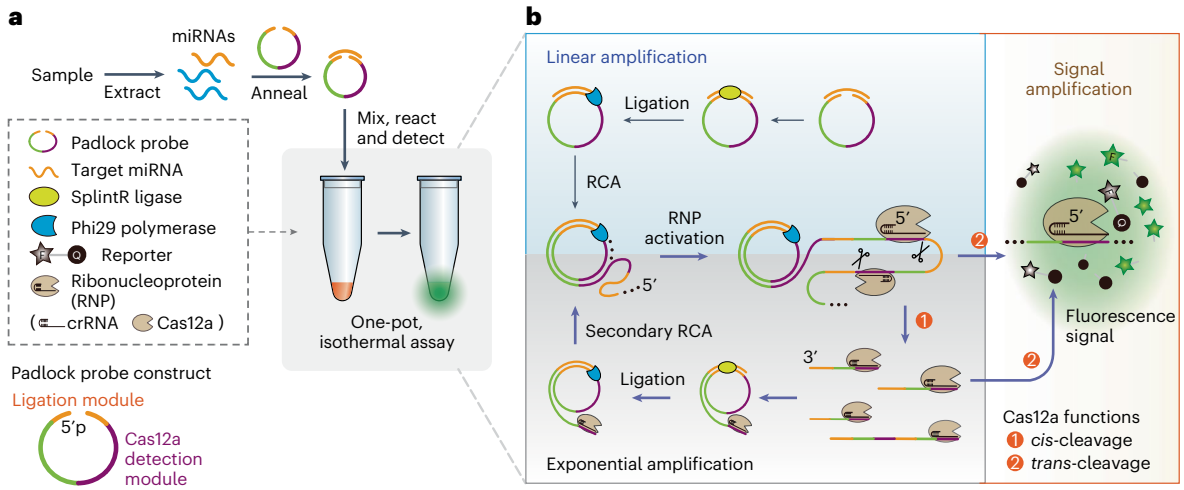


Fig. 1 | The one-pot EXTRA-CRISPR miRNA assay. a, The major components and workflow of EXTRA-CRISPR assay. The padlock probe for RCA is engineered with a split ligation module for target miRNA binding and a CRISPR–Cas12a detection module whose complementary sequence activates a Cas12a–crRNA complex. miRNA sequences are extracted from a sample, annealed with the padlock and then added to a reaction tube containing the enzymes, reporter and other reagents. The one-pot assay is carried out at 37 °C in a qPCR apparatus for real-time detection of the fluorescence signal. **b**, The proposed mechanism of the EXTRA-CRISPR. This assay harnesses both *cis*-cleavage and *trans*-cleavage functions of the CRISPR–Cas12a system to convert linear RCA to an exponential amplification method for miRNA detection. Briefly, the Cas12a RNP can bind and cleave the long ssDNA amplicon of RCA by its *cis*-activity, which generates many secondary primers containing the target sequence to initiate subsequent RCA cycles, resulting in exponential amplification of the target. Meanwhile, the amplicon-activated Cas12a RNP non-specifically cleaves the ssDNA reporters to create and amplify fluorescence signal.

and LAMP, and the relatively slow kinetics and low sensitivity of hybridization chain reaction and catalytic hairpin assembly. Other standard technologies such as microarrays[23], NanoString[24] and sequencing[25] offer powerful tools for highly multiplexed miRNA profiling with high throughput and flexibility[26,27]. However, these methods demand sophisticated instruments or have complex analytical workflows, high operational cost and limited analytical performance, which hinder their widespread applications to clinical diagnostics, especially for point-of-care (POC) testing.

Recently, CRISPR (clustered regularly interspaced short palindromic repeats) technologies have emerged as a versatile tool for developing the next-generation bioassays that combine the analytical performance of PCR and the ease of isothermal amplifications. The CRISPR–Cas12a and CRISPR–Cas13a systems confer highly specific target recognition via binding with the Cas enzyme–crRNA complex and enzymatic signal amplification owing to collateral cleavage (*trans*-activity) of a fluorogenic probe by the Cas enzyme activated upon target binding[28,29]. A variety of CRISPR assays have been reported for DNA and viral RNA detection which normally require an additional PCR or isothermal pre-amplification step to achieve desirable detection sensitivity[30–33]. Following the same strategy, sensitive CRISPR-based miRNA assays were also developed by incorporating pre-amplification of miRNA targets by various isothermal reactions, including RCA[34–36], LAMP[37] and cascade amplification[38]. However, these methods involving two separate pre-amplification and CRISPR-mediated readout steps require multi-step manual operations, which not only leads to complicated assay workflow and extended turnaround time but also increases the risk of analytical variations and false results due to human error, enzymatic degradation and cross-contaminations. It was recently demonstrated that it is possible to combine isothermal amplification and CRISPR detection in a one-pot reaction via delicately engineering the primer designs and reaction conditions[32,39–41]. However, it remains unclear whether such a strategy can be adapted to develop one-step, one-pot CRISPR assays for miRNA sensing. Alternatively, CRISPR-mediated target recognition can be integrated with other signal transduction modalities, such as electrochemical[42], plasmonic[43] and graphene field-effect transistor sensors[44], enabling amplification-free nucleic acid detection. However, these approaches are not truly comparable to RT-qPCR, due to either low sensitivity without pre-amplification[42] or the limitations arising from highly specialized devices and instruments needed. Lastly, it is worth noting that most, if not all, of the existing CRISPR-based methods leverage on the *trans*-cleavage activity of Cas proteins, while the exploration of the specific *cis*-cleavage activity—the main mechanism of CRISPR–Cas systems for gene editing—for biosensing remains largely untapped.

In this Article, we report a one-step, one-pot isothermal CRISPR–Cas12a assay, which we named 'Endonucleolytically Exponentiated Rolling Circle Amplification with CRISPR–Cas12a' (EXTRA-CRISPR) for the rapid and specific detection of miRNAs with sensitivity comparable to RT-PCR (Fig. 1). The EXTRA-CRISPR assay offers three major distinctions from the existing CRISPR-based biosensing methods. First, it represents a strategy to simultaneously harness both *cis*-cleavage and *trans*-cleavage activities of the CRISPR–Cas12a system. It exploits the specific *cis*-cleavage activity to transform conventional linear RCA to enable exponential amplification of target sequences, in addition to the *trans*-cleavage reaction for amplicon detection and signal amplification. Second, by engineering a modular padlock probe design and the reaction kinetics, we incorporate multiple reactions for target-mediated ligation, RCA, Cas12a binding and nucleolytic cleavage into one collaboratively coupled reaction network, creating a robust one-step, single-tube isothermal assay for miRNA analysis. Third, this one-pot isothermal miRNA assay affords comparable analytical performance with standard RT-qPCR, including high sensitivity with a single-digit femtomolar detection limit, single-nucleotide specificity and rapid and flexible turnaround (from 20 min to 3 h for the entire analysis depending on targets and samples). Lastly, one-pot EXTRA-CRISPR technology vastly simplifies the assay workflow and negates the need for specialized instruments, which provides an adaptable modality for POC diagnostics.

As proof of concept of potential applications, we adapted the EXTRA-CRISPR assay to quantifying miRNA biomarkers in extracellular vesicles (EVs) for the liquid-biopsy-based diagnosis of pancreatic ductal adenocarcinoma (PDAC). EVs, including exosomes of 50–150 nm in size, are emerging as a promising candidate for liquid biopsy because

they selectively sort and transport cellular cargoes, such as proteins and nucleic acids, that mirror the physiological and pathological states of parental cells[45–50]. EVs are considered a major carrier of miRNAs in human biofluids, and tumour-derived EVs offer a promising route to explore disease-specific miRNA signatures[45–52]. Using EXTRA-CRISPR, we show the highly sensitive and specific profiling of a panel of four miRNA markers (miR-21, miR-196a, miR-451a and miR-1246) in EVs derived from cell lines and clinical plasma specimens. Based on the individual EV-miRNA tests, an EV signature (EV-Sig) was devised with a machine-learning method to improve the diagnostic performance for pancreatic cancer. The analytical and diagnostic performance of the EXTRA-CRSPR tests were rigorously validated by parallel RT-qPCR analysis of the same clinical samples. These results suggest that the technology may help advance miRNA detection and the clinical development of miRNA biomarkers for liquid biopsy-based cancer diagnosis and prognosis.

Results

Mechanistic studies of the EXTRA-CRISPR assay

The assay is designed to be a tri-enzymatic cascade that exploits the unique nucleolytic cleavage activities of the CRISPR–Cas12a system to create a new exponential isothermal amplification mechanism based on the robust linear RCA assay. The assay starts with the hybridization of a padlock probe with the miRNA target in the one-pot reaction, which can be further enhanced by adding a rapid denaturing and annealing step in the sample preparation process before analysis, as illustrated in Fig. 1a. The padlock probe is a 5′-phosphorylated single-strand DNA engineered to encompass two modular sequences: a ligation zone bridging the 5′ and 3′ termini with the complementary sequence to target miRNA and a detection zone whose complementary sequence can be recognized by Cas12a–crRNA ribonucleoprotein (RNP) complexes. Upon mixing with all other assay reagents in a tube, the target-splinted padlock probe will be ligated with the SplintR ligase to form a circular template for isothermal RCA reaction. Driven by phi29 DNA polymerase, RCA continuously extends target miRNA to a long linear concatemer with repeatedly complementary copies of the padlock. The Cas12a RNP pre-formed in the solution will bind to the detection zones on the long concatemer, which activates the *trans*-cleavage activity of Cas12a enzyme to non-specifically cut the fluorophore quencher-labelled single-stranded DNA (ssDNA) reporters to produce fluorescence signal (Fig. 1b). In the meantime, the activated RNP can also cut the linear RCA product into short fragments via its *cis*-cleavage function. These fragments contain single or multiple complementary copies of the padlock and thus can serve as new primers to trigger many secondary RCA reactions. Such collaboratively coupled linear DNA polymerization and Cas12a *cis*-cleavage can be repeated continuously to generate the chain reactions converting conventional linear RCA to an exponential amplification assay (Fig. 1b). The post-cleavage RNP complexes may also cause collateral cut of the ssDNA reporters and thus further promote CRISPR signal amplification to enhance the detection sensitivity.

The development and mechanistic studies of EXTRA-CRISPR were conducted using miR-21 as the model target, which has been found overexpressed in various human tumours[53]. The key module in our padlock probe design, the CRISPR detection zone, was verified by detecting its complementary strand with a CRISPR–Cas12a-only assay. A limit of detection (LOD) at the 1 pM level was obtained (Supplementary Fig. 1), in line with the reported performance for preamplification-free CRISPR–Cas detection[31,42]. The EXTRA-CRISPR assay is expected to produce both single-stranded RCA amplicon and the amplicon–padlock duplex both containing the crRNA-complementary sequences. RNA-guided binding with a double-stranded DNA activator requires a protospacer-adjacent motif (PAM) to activate Cas12a for both specific *cis*-cleavage and effective non-specific ssDNA *trans*-cleavage, whereas a ssDNA does not need the PAM but yields less catalytic activity for *trans*-ssDNA cutting[31]. Hence, we first examined the effects of CRISPR–Cas12a in our one-pot assay by tuning its activities with the PAM sequence in the padlock. As shown in Fig. 2a, the PAM-free padlock-1 resulted in a considerably higher reaction rate and signal level compared with padlock-2 with a PAM sequence, indicating an inhibitory effect of the PAM in the padlock for our one-pot assay. This result implies the importance of establishing proper equilibrium among the RCA and CRISPR–Cas12a cleavage reactions to catalyse efficient target amplification for which a PAM-free padlock is preferred, as further examined below.

To facilitate the mechanistic studies, we first conducted the EXTRA-CRISPR reactions with padlock-1 at high miR-21 concentrations (1 pM to 1 nM) to permit both real-time fluorescence detection and gel electrophoresis analysis of the reaction products. Figure 2b shows that our tri-enzyme assay enormously increases the detection signal with 1 pM miR-21 compared with the Cas12a-only detection (Supplementary Fig. 1). In the control reactions with one of three enzymes left out each time, no fluorescence signal was detected, verifying the essential role of each enzyme in the one-pot EXTRA-CRISPR system. The signal intensity was observed to rise with the miR-21 concentration increased to 10 pM but then to largely decrease at 100 pM and 1 nM (Fig. 2b), indicating the dynamic coupling of competing reactions associated with Cas12a in this tri-enzyme assay. The products of these reactions were analysed with agarose gel electrophoresis. In the absence of Cas12a RNP, a band of high-molecular-weight DNA was detected at the edge of the sample wells, and the DNA amount increased with the miR-21 input (Fig. 2c), which confirms successful miR-21 amplification by ligation-assisted RCA. No cleaved reporter was detected on the gel, consistent with the negative fluorescence detection seen in Fig. 2b. With RNP added, the one-pot reaction at a relatively low miR-21 concentration (1–100 pM) resulted in a barely detectable band of long RCA product and a weak band of small-molecular-weight DNA (Fig. 2c, lanes 1, 3 and 5), which can be presumably attributed to relatively complete cleavage of long DNA product by the activated RNP. In addition, a clear fluorescent gel band of collaterally cleaved reporter by Cas12a was detected with the intensity being enhanced at the target concentration of 10 pM and then largely reduced at 100 pM (Fig. 2c, lanes 1, 3 and 5), which agrees with the real-time detection results (Fig. 2b).

When the miR-21 concentration was further increased to 1 nM (Fig. 2c, lane 7), the long RCA amplicon was clearly detected, excluding the inhibition of RCA reaction as the main factor for signal suppression observed at high target concentrations. The band of long RCA amplicon was much weaker than that for the RNP-free reaction (Fig. 2c, lane 8) and largely smeared, which verifies Cas12a cleavage of the RCA product. Compared with the cleaved DNA bands observed for the lower target concentrations, the broad smearing indicates much less effective cleavage by the excessive DNA amplicon produced with 1 nM miR-21. While the activated Cas12a can cause both *cis*-cleavage and *trans*-cleavage of the RCA amplicon, the observed smearing bands should be mainly from the *trans*-cleavage product, because our standard gel electrophoresis assay was not sensitive enough to detect the low-level *cis*-cleaved DNA produced with 1 nM of RNP. Moreover, the cleaved-reporter band became indiscernible when the target concentration increased to 1 nM (Fig. 2c). Such competitive cutting of reporter versus RCA amplicon can be attributed to the non-specific ssDNase activity of Cas12a that leads to preferential cut of the RCA amplicon when a high target input initiates extremely fast RCA reaction to produce considerably more ssDNA products than the reporter. The competing effect of Cas12a *trans*-activity was verified by conducting a simple ssDNA cleavage reaction in which a transition from the reporter-dominant to padlock-dominant cleavage was observed upon the descending reporter-to-padlock ratio (Supplementary Fig. 2). In our assay, the padlock concentration is only 1/10 of the reporter, and thus the padlock degradation by Cas12a *trans*-cutting should have minuscule effect on the EXTRA-CRISPR reaction. Together, these results suggest that our assay can produce a favourable RCA amplicon-to-reporter ratio over a broad range of target input (up to

https://doi.org/10.1038/s41551-023-01033-1

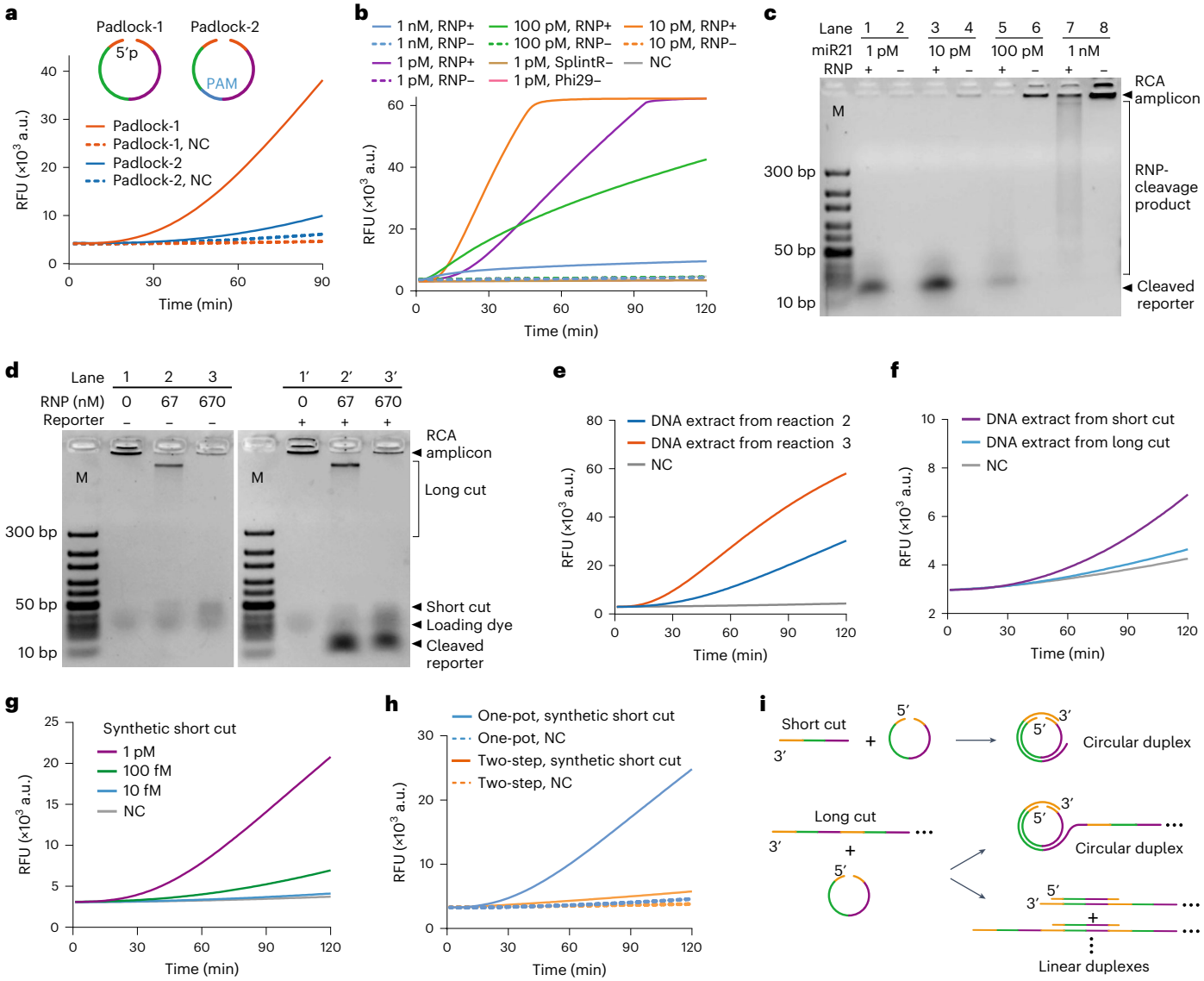


Fig. 2 | Mechanistic studies of EXTRA-CRISPR. a, Effect of the padlocks without and with a PAM sequence on miR-21 detection. The assays were conducted with 1 pM miR-21 and 100 nM of each padlock probe. NC, negative control assay with a buffer blank. RFU, relative fluorescence units. **b**, Real-time one-pot detection of serial 10-fold dilutions of miR-21 from 1 pM to 1 nM with 1 nM Cas12a RNP. Control assays were conducted with one of three enzymes left out each time. **c**, Gel analysis of the products from the reactions in **b**; an image of the full scans is provided in Source Data. **d**, Assessment of Cas12a activities on RCA amplicons in a two-step fashion. In this case, ligation–RCA was first conducted, and then the products were treated with varying amounts of RNP. M, DNA marker; an image of the full scans is provided in Source Data. **e**, EXTRA-CRISPR assays using the cleaved RCA products from reactions 2 and 3 in **d** as the targets. **f**, EXTRA-CRISPR detection of the long-cut and short-cut extracts recovered from the gel bands in lane 2 in **d**. Despite its lower quantity, the short-cut extract yielded a faster reaction kinetics than the long-cut extract. **g**, Synthetic ssDNA mimicking the short-cut RCA product effectively triggers the EXTRA-CRISPR assay to produce quantitative signals. **h**, Exponential amplification of this synthetic short cut was observed in the one-pot assay, as opposed to linear amplification of the synthetic short cut in the two-step assay. The target concentration in both cases is 1 pM. **i**, Illustration of the length-dependent binding of the Cas12a-cleaved RCA amplicons that results in differential efficiency for the secondary ligation and RCA reactions. In contrast to the short-cut amplicon, the long cuts may hybridize with the padlock sequences in the linear forms, which terminates the ligation and exponential RCA.

~100 pM, equivalent to 10^9 copies per 20 µl reaction), enabling quantitative *trans*-cleavage of the fluorogenic reporter for accurate miRNA detection.

For comparison, the experiments for 1 pM to 1 nM miR-21 discussed above were repeated with padlock-2. As presented in Supplementary Fig. 3a, the observed reaction kinetics appeared to be much slower than that with padlock-1 (Fig. 2b), and accordingly, notable amplification suppression occurred at a higher miR-21 concentration (1 nM versus 100 pM). Gel analysis of these reactions (Supplementary Fig. 3b) detected a pattern of RNP-cleavage products and cleaved reporter similar to that obtained with padlock-1 (Fig. 2c). Consistent with the real-time fluorescence detection, the gel bands of cleaved reporter were much weaker than that for padlock-1, verifying the inhibitory effect of the PAM on the amplification efficiency of our one-pot assay. This effect can be presumably attributed to the PAM-mediated RNP binding with the amplicon–padlock duplexes that activates both *cis*-cutting of the circular templates for RCA and rapid non-specific degradation of all ssDNA species including the cleaved amplicons for the secondary RCA[31,39,54]. Indeed, compared with the padlock-1 reaction (Fig. 2c), the padlock-2 reaction was seen to produce relatively strong gel bands of low-molecular-weight RNP-cleavage products with respect to the reduced bands of cleaved reporter. Overall, this comparative

study should support the essential role of the engineered PAM-free padlock-1 in tuning the dual reactivities of CRISPR–Cas12a to drive exponential RCA of miRNA.

To further assess the Cas12a reactivities in the EXTRA-CRISPR reaction, we conducted a two-step assay in which the ligation-assisted RCA was first performed, followed by treating the amplicon with Cas12a RNP of variable concentrations. The reactions were run with the high concentrations of miR-21 (1 nM) and RNP (up to 670 nM) to facilitate the detection of both *cis*-cleaved and *trans*-cleaved DNA products. Figure 2d shows that when 67 nM RNP was used, the long DNA amplicon produced by RCA (lanes 1 and 1′) were partially cleaved to yield a smeared band of long fragments and a band of short fragments (lanes 2 and 2′) which are thereafter referred to as the long and short cuts, respectively. This observation indicates enhanced cleavage of the RCA amplicon by more RNP in comparison with the assay shown in Fig. 2c (lane 7). Increasing the RNP concentration to 670 nM led to apparently complete digestion of the long cut into the short cut (lanes 3 and 3′). At these high levels of RNP over ssDNA substrate, the bands of *trans*-cleaved reporter were also detected (Fig. 2d, lanes 2′ and 3′), which is consistent with the observations for the one-pot reactions in which low levels of RCA amplicon were produced (Fig. 2c, lanes 1–4). A distinct observation in the two-step reactions with high-concentration RNP was an intense band of long cut (Fig. 2d, lanes 2 and 2′) that was barely detectable with the low level of RNP (Fig. 2c, lane 7). We hypothesized that this intense long-cut band is mainly produced by the *cis*-activity of RNP, and thus the short-cut band should also contain a considerable amount of the small fragments of *cis*-cleaved RCA amplicon. These *cis*-cleavage products contain complementary copies of the padlock and may serve as new primers for secondary RCA reactions to initiate exponential amplification of target miRNA. To test our hypothesis, we investigated the ability of CRISPR-cleaved RCA products to exponentiate the linear RCA reaction. As the ssDNA amplicon of RCA is chemically different from miRNA, we first verified that the DNA version of miR-21 yields comparable amplification efficiency with miR-21 for the EXTRA-CRISPR reaction (Supplementary Fig. 4). We performed the EXTRA-CRISPR assays using the DNA extracted from the two-step reactions tested in Fig. 2d as the target. As seen in Fig. 2e, notably higher amplification was obtained with the DNA extract that contained mostly the short cut (Fig. 2d, lane 3) than that containing both short and long cuts (Fig. 2d, lane 2).

To further examine such differential reactivity of *cis*-cleaved RCA products, we extracted DNA from the separated gel bands of the short and long cuts in lane 2 of Fig. 2d and input them as the targets for the EXTRA-CRISPR assays. Despite its larger quantity as detected on gel, the long-cut extract appeared to weakly trigger the tri-enzymatic reaction, while the short cut yielded much faster reaction kinetics and higher amplification signal (Fig. 2f). The low molecular weight of the short-cut band observed on gel suggests that the *cis*-cleaved fragments in the band roughly correspond to one monomeric unit of the RCA concatemer with a length of 61 nucleotides (Supplementary Table 1). Thus, we assessed a synthetic ssDNA of the unit sequence as the input for the EXTRA-CRISPR reaction. Figure 2g shows the quantitative titration of this synthetic short-cut mimic down to a concentration of 10 fM, >100-fold lower than the LOD of the preamplification-free Cas12a assay (Supplementary Fig. 1). The one-pot assay with the synthetic short cut was seen to yield notably higher signal intensity than the two-step assay involving linear amplification of the synthetic short cut at the same concentration (1 pM, Fig. 2h), indicating the high efficiency of the short cut to trigger exponential RCA. Collectively, these results should verify the major contribution of the short *cis*-cleaved amplicon to exponentiating linear RCA over the long *cis*-cleaved ones, which may be explained by their length-dependent binding with the padlock probe as depicted in Fig. 2i. The unit sequence only binds with the termini of a padlock to form a circular duplex that initiates the exponential amplification. By contrast, the *cis*-cleaved long fragments may cause two competing effects via: (1) circularizing the padlock with the 3′ end complementary site to initiate RCA and (2) hybridizing the padlock probes with other binding sites to form linear duplexes, which leads to the termination of exponential reaction. A long fragment has more padlock binding sites along the strand than at the terminal, and thus the probability to form linear duplexes is higher than that for forming circular probes. Therefore, the ability of long-cut fragments to initiate exponential RCA can be largely suppressed (Fig. 2f). Overall, our findings show dynamic coupling of the *trans*-cleavage and *cis*-cleavage activities of Cas12a in the EXTRA-CRISPR assay, which enables exponential amplification of the target.

One-pot chemistry amplifies the performance of stepwise combined reactions

To directly assess the impact of dual-activity CRISPR on the tri-enzyme reaction network, we compared miR-21 detection using the ligation-assisted RCA, tandem RCA and CRISPR, and one-pot EXTRA-CRISPR assays, under otherwise the same reaction conditions (Methods). The conventional assay composed of two sequential reactions of ligation and RCA affords a high LOD at the ~100 pM level for miR-21 (Fig. 3a). Tandem combination of RCA amplification with the specific and powerful Cas12a-based signal amplification vastly improved the sensing sensitivity to detect miR-21 below 100 fM (Fig. 3b), which is in line with the performance reported with a similar three-step RCA-Cas12a assay[36]. Based on this three-step tandem assay, we tested a simplified version that combines ligation and RCA in one pre-amplification reaction followed by the Cas12a-powered fluorogenic readout. While simplifying the workflow, this two-step RCA-CRISPR–Cas12 approach appeared to slightly compromise the detection sensitivity and speed as indicated by the lower signal detected over a longer reaction time (Fig. 3c). This can be because the reaction conditions optimized for one enzyme may be suboptimal for others and, thus, the overall system. In contrast, our one-pot assay was able to overcome this challenge and confer sensitive detection of as low as 10 fM miR-21 using a protocol yet to be optimized, which notably outperforms the three-step assay based on linear RCA (Fig. 3d).

Given that the isothermal assays investigated here combine continuous RNA replication and fluorogenic signal amplification, we evaluated their overall amplification efficiency by quantifying the number of fluorescent probes produced per input miRNA template (equivalent to amplification fold), as depicted in Supplementary Fig. 5. The two-step RCA-CRISPR assay was estimated to yield 5.8×10^4-fold and 5.9×10^4-fold amplification at the 10 fM and 100 fM miR-21 input in 2 h, respectively. These values are higher than the amplification efficiency of linear RCA by phi29 polymerase which was previously reported to be ~1,000–2,000 replicates of one circular template per hour, owing to the Cas12a-based signal amplification[55–57]. The overall amplification efficiency for the EXTRA-CRISPR assays with 10 fM and 100 fM miR-21 was estimated to be 1.6×10^6 and 1.7×10^6 6-Carboxyfluorescein (FAM) probes per template, respectively, which is ~30-fold higher than that of the two-step assay. It is worth noting that such comparison of the overall amplification efficiency may largely underestimate the miRNA replication efficiency of our one-pot assay over the two-step assay, because the signal-generation reaction in the one-pot assay occurs with the Cas12a target that increases from a very low level over the 2 h reaction, while in the two-step assay the second reaction for signal generation starts with a vast quantity of the Cas12a target produced by the first RCA step. Overall, these comparative studies of different assay modes support the collaborative coupling of *trans*-activities and *cis*-activities of CRISPR–Cas12a in our assay to drive exponential RCA and fluorogenic signal amplification simultaneously. The dynamics of the coupled tri-enzyme reaction can be affected by several major factors, which were systematically optimized as detailed below.

Optimization and characterization of the EXTRA-CRISPR assay

As discussed above, our padlock probe is engineered with a CRISPR detection module which guides RNP *cis*-cleavage of RCA amplicon to

https://doi.org/10.1038/s41551-023-01033-1

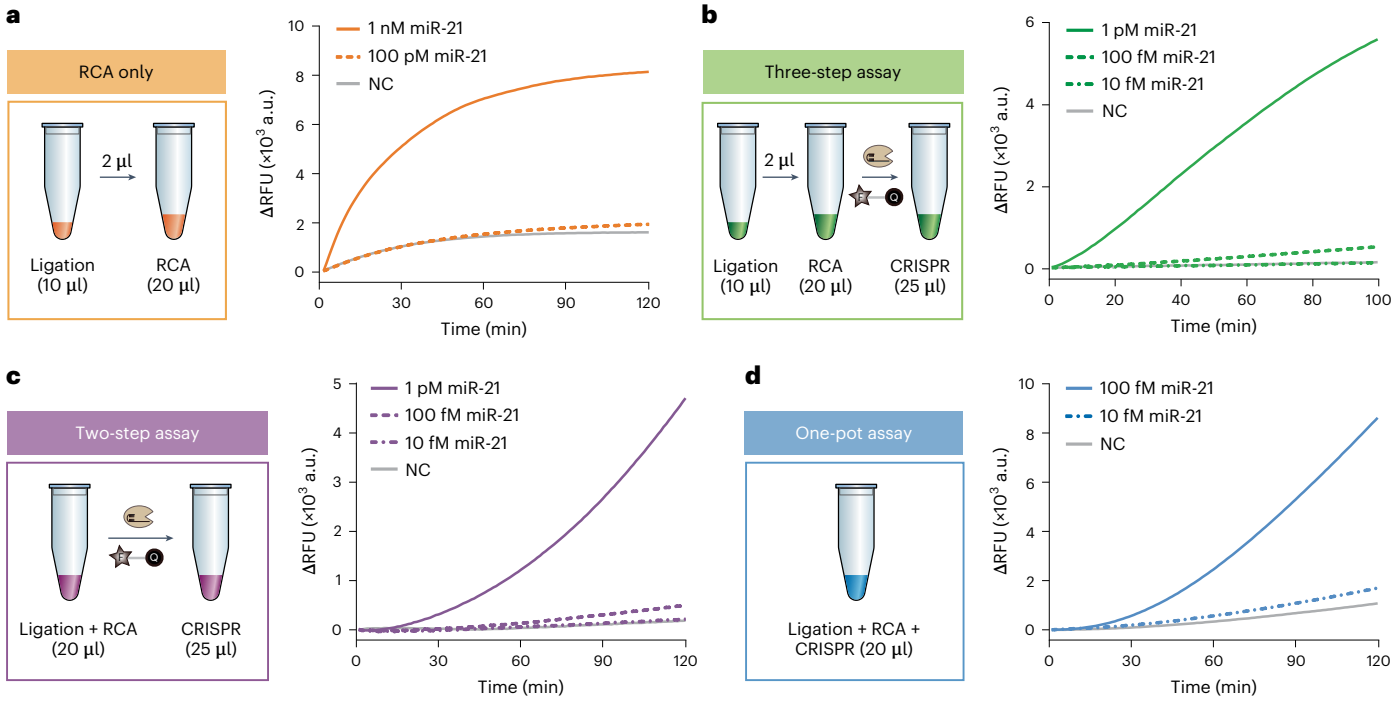


Fig. 3 | Comparison of the kinetics and detection sensitivity of RCA, one-pot EXTRA-CRISPR and multi-step CRISPR-assisted RCA assays. a, The RCA-only method involves two sequential reactions of ligation and linear RCA and can only detect 100 pM miR-21. Ligation condition, 100 nM padlock probe and 0.625 U μl^{-1} SplintR ligase. RCA condition, 2 μl ligation product, 0.2 U μl^{-1} phi29 and SYBY Green II for detection. **b**, The assay that connects three tandem steps of ligation, RCA and Cas12a readout yielded a LOD of ~100 fM. The conditions for ligation and RCA were the same as in **a**. After RCA and denaturing of enzymes, 40 nM RNP and 0.8 μM reporter were added into the reaction. **c**, In the two-step method, ligation and RCA were combined together, followed by fluorogenic detection using Cas12a RNP, conferring similar sensitivity with the three-step assay in **b**. **d**, The one-pot EXTRA-CRISPR method improves the sensitivity to detect 10 fM miR-21 before full optimization. Assay concentrations used in **c** and **d**, 100 nM padlock-1, 0.625 U μl^{-1} SplintR ligase, 0.1 U μl^{-1} phi29 polymerase, 1 μM reporter and 1 nM Cas12a RNP.

generate new primers for secondary RCA. Moreover, insertion of this critical module affects the overall sequence of padlock probe that is an important factor governing the efficiency of ligation and RCA reactions[58–60]. To assess these effects and optimize the padlock probe design, we constructed three padlock probes with the CRISPR detection zone located in the right (padlock-1), middle (padlock-3) and left (padlock-4) of the sequence. As shown in Fig. 4a, padlock-1 constantly generated the highest detection signal and the lowest background level over an hour of reaction, indicating its advantage to enact efficient and specific EXTRA-CRISPR reactions. We speculate that such effect may arise from the undesired secondary structures of the padlock probes that reduce the hybridization affinity and specificity for ligation and RCA, because oligonucleotide analysis showed that padlock-3 and padlock-4 can form more stable hairpins. To further test these effects, we designed a set of variants of padlcock-1 by modifying the sequence outside the ligation and detection modules to intentionally induce more complex and stable hairpin structures and self-dimers (Supplementary Fig. 6). Compared with the original padlock-1 design, padlock-1-1 with three modified nucleotides resulted in a largely reduced amplification signal and higher non-specific background. With more nucleotides altered to form increasingly stable hairpin and self-dimer structures, these variants led to deteriorating signal-to-background ratio, complete inhibition of specific amplification (padlock-1-3) and even worse non-specific background (padlock-1-4). These results confirm the remarkable impact of the secondary structures of padlock probe on the one-pot reaction. There are other possible effects associated with the location of the detection zone, such as the steric hindrance that can affect the binding of three enzymes onto the circular template–padlock complexes.

Ligation of the padlock annealed to a miRNA splint is the initiating enzymatic reaction in the EXTRA-CRISPR cascade. Compared with DNA–DNA helices, RNA-splinted hybrid helices are known to be much less efficient substrates for DNA ligases, including T4 DNA ligase that is widely used in RCA assays[59]. To obtain an efficient ligation reaction, we compared T4 DNA ligase and the PBCV-1 DNA ligase, also commercially branded as SplintR ligase, which was reported to provide a much higher affinity (~300-fold Michaelis constant K_M) and turnover rate (20-fold catalytic rate constant k_{cat}) for RNA-splinted DNA substrates[59]. T4 DNA ligase appeared to be ineffective to trigger the one-pot assay, whereas SplintR ligase substantially expedited the reaction kinetics and enhanced the signal intensity (Fig. 4b), indicating the importance of ligation to the overall reaction kinetics and efficiency. In addition, SplintR ligase confers good stability in the assay performance over a 20-fold change of enzyme quantity (2.5 to 50 units per reaction, Supplementary Fig. 7). To further optimize the ligation reaction, we investigated the enhancement of miRNA–padlock probe hybridization by a quick denaturing and annealing step (Fig. 1a) which is a commonly practiced sample treatment method to promote nucleic acid hybridization in bioassays. As expected, this additional pre-treatment of RNA samples by 5 min denaturing and ~1 min annealing improves the amplification efficiency while reducing the non-specifical background, compared with the original assay protocol (Supplementary Fig. 8). The denaturing step was found to remain effective when shortened to 10 s (Supplementary Fig. 9). Nevertheless, our final workflow implements the 6 min pre-treatment step to ensure the consistent assay performance without notably extending the total turnaround time.

Next, we attempted to optimize the major RCA-related components for the EXTRA-CRISPR assay. It was found that Cas12a RNP can work effectively in the SplintR buffer with bovine serum albumin (BSA) (Supplementary Fig. 10a) and the SplintR buffer greatly outperforms the phi29 buffer (Supplementary Fig. 10b). BSA was found to be a

https://doi.org/10.1038/s41551-023-01033-1

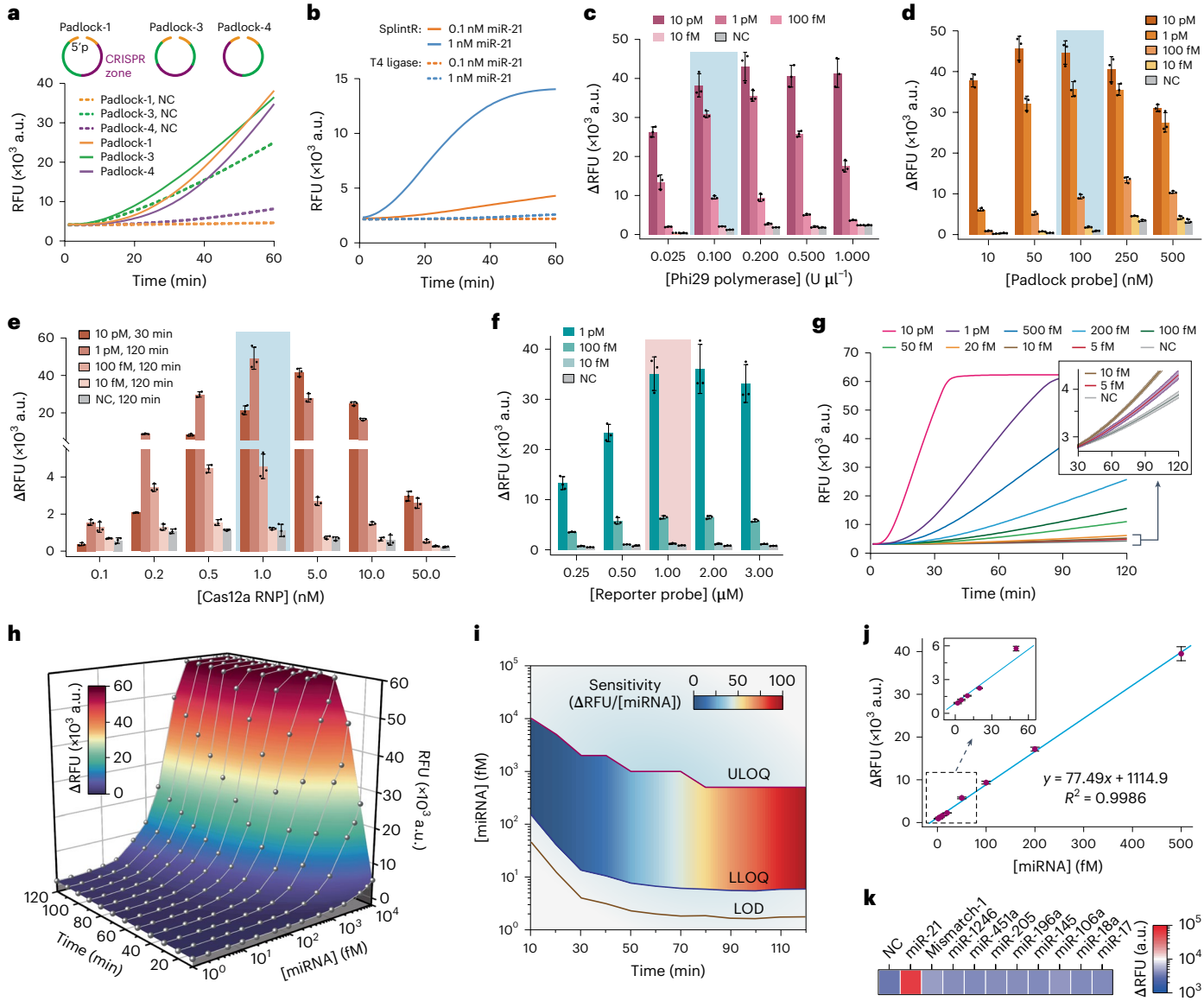


Fig. 4 | Optimization of the one-pot EXTRA-CRISPR miR-21 assay. a, The position of the CRISPR module in a padlock sequence affects the detection signal and background level. The assays were conducted with 1 pM miR-21 and 100 nM padlock. **b**, Comparison of T4 DNA ligase and SplintR ligase for the one-pot assay. The assays were conducted with 40 U μl^{-1} T4 DNA ligase or 2.5 U μl^{-1} SplintR ligase, 100 nM padlock-1, 0.2 U μl^{-1} phi29 polymerase, 50 nM Cas12a RNP and 1 μM reporter. **c**–**f**, Optimization of the concentration of phi29 (**c**), padlock (**d**), Cas12a RNP (**e**) and reporter (**f**). ΔRFU, unless otherwise specified, was the signal increase from 0 min to 120 min. Error bars, 1 s.d. ($n = 3$). The selected optimal conditions are indicated by a colour background. **g**, Representative real-time curves for calibrating the one-pot assay with serial dilutions of synthetic miR-21 standards using the optimized protocol. Inset: the curves of averaged signal for 0 fM (NC), 5 fM and 10 fM miR-21 with the shaded bands indicating 1 s.d. ($n = 5$). **h**, Titration curves plotted at various time points for the assay calibration in **g** show a strong dependence of the assay performance on the reaction time. **i**, Diagram of the analytical figures of merit determined by the assay calibration, including LOD, sensitivity (the slope of linear calibration curve) and linear dynamic range defined by the lower limit of quantification (LLOQ) and upper limit of quantification (ULOQ). **j**, Linear calibration obtained with the optimal assay time of 100 min yields a LOD of 1.64 fM miR-21 calculated from 3 × s.d. of the background level and a linear range from 5.47 fM to 500 fM. Error bars, 1 s.d. ($n = 5$). **k**, Specificity of the EXTRA-CRISPR for detecting miR-21 against a single-mismatch miR-21 sequence (mismatch-1) and eight different miRNAs (1 pM each). The colour intensity represents the averaged signal level of two replicates.

critical additive that can effectively augment the amplification efficiency in a proper concentration range (0.1–0.3 mg ml^{-1}, Supplementary Fig. 11). Two additional additives previously used to promote SplintR ligation, Mn^{2+} ion[59] and ssDNA binding protein (SSB)[61], were tested as well. Mn^{2+} ion appears to substantially increase non-specific background (Supplementary Fig. 12), while adding SSB tends to suppress the EXTRA-CRISPR reaction (Supplementary Fig. 13); hence, Mn^{2+} ion and SSB are not used in the following optimizations. We then optimized the phi29 polymerase concentration which is a key factor to achieving the balanced RCA and CRISPR–Cas12a cleavage reactions to catalyse exponential amplification, as reasoned before. Similar to the effect of miRNA input (Fig. 2c), increasing the quantity of phi29 polymerase will promote RCA reaction to generate higher detection signal, but excessive RCA amplicon can suppress *trans*-ssDNA cutting of reporter by RNP, resulting in reducing signal intensity. The presence of an optimal polymerase concentration was experimentally observed, which showed a shift to the higher level for lower miRNA input (Fig. 4c). Similar peaking behaviour was observed for the padlock probe as well because higher padlock concentration can enhance the efficiency for target binding and subsequent RCA (Fig. 4d). Given the low abundance of miRNAs in many biological samples, including EVs, we selected the optimal concentrations of 0.1 U μl^{-1} and 100 nM for phi29 polymerase

and the padlock, respectively, which yielded the highest signal against the background for the range of 10 fM to 1 pM miR-21.

Optimization of the CRISPR components in the one-pot reaction started with assessing Cas12a RNP at a typical concentration of 50 nM used in the standard Cas12a assays[31]. However, this established assay condition led to poor signals for our assay (Fig. 4e), because excessive RNP can cause a termination effect, that is, *cis*-cleavage of RCA amplicon–padlock duplexes and non-specific *trans*-cutting of the padlock, reducing the efficiency of both target amplification and fluorogenic CRISPR readout (Fig. 2). Thus, we screened a wide range of Cas12a RNP concentration from 0.1 nM to 50 nM to find a condition that maximizes the desired catalytic effect against the adverse termination effect of CRISPR–Cas12a in the one-pot EXTRA-CRISPR. As expected, the assay signal showed a peaking trend as a function of the RNP concentration depending on the target input, and the optimal range was narrowed down to 0.5 nM to 1 nM for the targeted miRNA concentration range of 10 fM to 1 pM (Fig. 4e). We have shown that indiscriminate ssDNase activity of Cas12a can not only cut the reporter but also degrade the padlock and linear RCA amplicon to inhibit the exponential amplification. Thus, increasing the reporter concentration would kinetically improve fluorogenic signal amplification and thermodynamically enhance the amplification efficiency by mitigating the inhibitory ssDNA cutting, while excessive reporter may raise the background signal. Indeed, the one-pot assay was seen to yield an ascending signal when the reporter concentration was increased from 25 nM to 1 μM (Fig. 4f). This effect was most substantial at the high miRNA input (1 pM), which is consistent with the observed competitive Cas12a *trans*-cutting of ssDNAs (Fig. 2c and Supplementary Fig. 2). With other optimized variables, we selected a combination of 1 nM RNP and 1 μM reporter to maximize the signal-to-noise ratio of our one-pot assay. Collectively, these optimization studies revealed the unique dynamics of our assay which corroborates synergistic coupling of the enzymatic reactions via harnessing the dual activities of CRISPR–Cas12a.

Lastly, the analytical performance of the EXTRA-CRISPR assay was systematically calibrated with serial dilutions of synthetic miR-21 using the optimized protocol. Figure 4g shows the typical curves for real-time detection over a reaction time of 2 h. The titration curves of signal versus concentration were also plotted at various time points, which show a strong dependence of the assay performance on the reaction time (Fig. 4h). To quantitatively evaluate the impact of reaction time on the assay performance, we computed the analytical figures of merit including LOD, sensitivity (the slope of linear calibration curve) and linear dynamic range defined by the lower limit of quantification and upper limit of quantification, which are graphically presented in Fig. 4i. With 20 min assay time, our method conferred a LOD of 12.3 fM which vastly outperforms the three-step assay[36] reporting a LOD of 34.7 fM with a total of 4.5 h for both RCA and Cas12a reactions (Supplementary Table 2). Extending the reaction time improves the LOD and shifts the linear dynamic range down until reaching a minimal LOD of 1.64 fM with a linear range from 5.47 fM to 500 fM (R^2 = 0.9986, Fig. 4j) at 100 min. Moreover, the calibration sensitivity of our assay can also be improved over time to better discriminate the small variations in target concentration.

It is seen that the signals obtained with high miR-21 concentrations (1–10 pM) saturate at a constant level (Supplementary Fig. 14a), indicating that the observed linear dynamic range of our assay could be limited by the fluorescence detector used in the qPCR machine. To test such instrumental limitation, we conducted the same assays using a commercial microplate reader with high sensitivity and a broad dynamic range. Indeed, the microplate reader yielded dynamic signal response with no saturation (Supplementary Fig. 14a), enabling quantitative detection with a linear range extended up to 10 pM miR-21 (Supplementary Fig. 14b). These results verify the instrumental limitation of the qPCR machine on the dynamic range of our assay and suggest the feasibility of achieving quantitative miRNA detection across a >4 log concentration range (from ~5 fM to 100 pM) via coupling our assay with a proper detector. Despite its limited dynamic range, we still chose to use the qPCR machine in the subsequent studies because it allows direct comparison between our method and the standard qPCR assays on the same instrument. The analytical performance of our assay was systematically validated by the parallel measurements with gold standard RT-qPCR. Our one-pot assay offers comparable detection sensitivity compared with a commercial miRCURY LNA miRNA PCR kit with which a LOD of 1.57 fM was obtained following the recommended two-step, 3 h protocol (Supplementary Fig. 15).

To assess the specificity of our method, we extended the miR-21 assay to detect a number of non-target miRNAs including a synthetic miR-21 with a single-nucleotide mismatch at the ligation site for padlock-1 (mismatch-1, Supplementary Fig. 16a) and eight human miRNAs at 1 pM each. These tests yielded a signal level of ~2% of the miR-21 signal or even lower (Fig. 4k), showing the excellent specificity of our assay. Such performance can be attributed to the multi-layered protection by the specific reactions for target–padlock hybridization, ligation[60], RCA and Cas12a activation and *cis*-cleavage[31]. We then investigated the effect of mismatch location on the assay specificity. As expected, the discrimination power was observed to be highest for the single mismatches located at the ligation site and reduced progressively with the increasing distance from the ligation site (Supplementary Fig. 16), owing to decreasing impact of single mismatches on the target–padlock hybridization. Phi29 polymerase might also contribute to the non-specific amplification when the single mismatches approach the 3′ terminus because its 3′→5′ RNase activity can digest the terminal mismatched nucleotides by proof-reading to restart polymerization[62]. A reasonably good specificity was still obtainable for a single mismatch shifted three nucleotides from the ligation point, with a non-specific signal level of ~25%. These findings show the importance of padlock design and optimization to afford the optimal single-base specificity. Moreover, we adapted our approach to detect a different target, miR-17, using four padlocks designed to differ in the 3′ end bases. Consistently, these single-mismatched padlocks yielded <2% non-specific signals with respect to the perfectly matched padlock (Supplementary Fig. 17). Overall, these results should validate the established one-pot EXTRA-CRISPR assay for rapid miRNA detection with single-digit femtomolar sensitivity and single-base specificity using a properly engineered padlock probe.

Quantitative profiling of EV-miRNAs for pancreatic cancer diagnosis

As a proof-of-concept demonstration of potential biomedical applications, we adapted the EXTRA-CRISPR assay to detect small EV (sEV) miRNAs for diagnosis of PDAC. To this end, both cell culture media and human plasma samples were used to isolate sEVs and extract short RNAs from the sEV preparations, followed by parallel measurements with the one-pot EXTRA-CRISPR and two-step RT-PCR assays (Fig. 5a). Previous studies have identified numerous EV-miRNAs associated with human PDAC, from which we selected four serum–plasma-derived EV-miRNAs that are frequently reported to be dysregulated in PDAC: miR-21[63–66], miR-196a[63,65,67–69], miR-451a[64,70–72] and miR-1246[67,73]. As described above for miR-21, three EXTRA-CRISPR assays were established to detect miR-196a, miR-451a and miR-1246 with a specific padlock probe, respectively (Supplementary Table 3). Figure 5b presents the calibration plots for detecting the three miRNAs by EXTRA-CRISPR from which the LOD was determined to be 1.35 fM (5–500 fM linear range, R^2 = 0.9974) for miR-196a, 4.14 fM (5–500 fM linear range, R^2 = 0.9992) for miR-451a and 7.96 fM (20–500 fM linear range, R^2 = 0.9984) for miR-1246. Consistent with the case for miR-21, these LODs were comparable with those of the standard RT-qPCR assays which were calculated to be 1.69 fM for miR-196a, 0.51 fM for miR-451a and 21.1 fM for miR-1246 from the calibration curves with a threshold Ct (cycle threshold) value of 35 (Fig. 5c and Supplementary Fig. 18). Our assays were also shown

https://doi.org/10.1038/s41551-023-01033-1

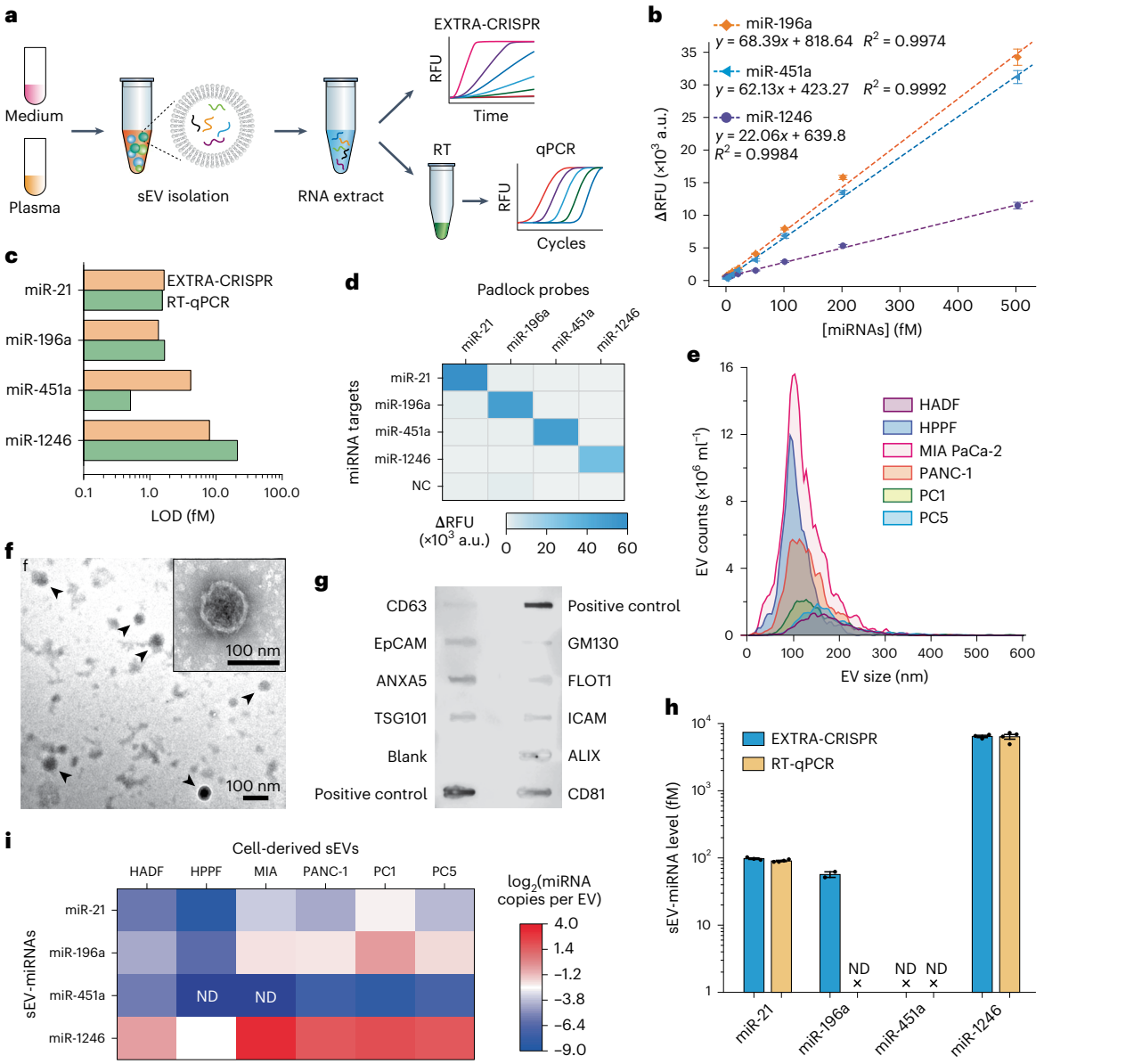


Fig. 5 | Quantitative profiling of EV-derived miRNAs. a, Experimental procedure for comparative analysis of miRNAs in EVs isolated from cell culture media and human plasma, respectively, using both EXTRA-CRISPR and RT-qPCR. **b**, Calibration curves for quantifying miRNA-196a, miR-451a and miR-1246 by EXTRA-CRISPR. Error bars, 1 s.d. ($n = 3$). **c**, Comparing the LODs for the EXTRA-CRISPR and RT-qPCR analyses of four miRNA targets. **d**, Validation of specific analysis across four miRNAs (1 pM each) by EXTRA-CRISPR. The colour intensity denotes the averaged signal level of three technical replicates for each target. **e**, Abundance and size distribution analyses of EVs isolated from serum-free media of six control and PDAC cell lines by NTA. Normal controls were HADF and HPPF; PDAC cell lines were MIA-PaCa-2, PANC-1, PC1 and PC5. **f**, Representative TEM images of PANC-1 cell-derived sEVs isolated by ultracentrifugation. Inset: spherical morphology of a sEV highlighting the lipid membrane structure. **g**, Quality assessment of isolated sEVs with a commercial antibody array. PANC-1 cell-derived sEVs were assayed to detect eight EV-associated protein markers, including CD81, CD63, FLOT1 (flotilin-1), ICAM1 (intercellular adhesion molecule 1), ALIX (programmed cell death 6 interacting protein), EpCAM (epithelial cell adhesion molecule), ANXA5 (annexin A5), TSG101 (tumour susceptibility gene 101) and a control for cellular contamination, GM130 (*cis*-golgi matrix protein); an image of the full scans is provided in Source Data. **h**, Comparison of the miRNA levels of MIA-PaCa-2 sEVs determined by EXTRA-CRISPR and RT-qPCR analyses of short RNA extracted from 30 µl of purified sEVs. Error bars, 1 s.d. ($n = 2$–4 as indicated). **i**, Heatmap of the normalized expression levels of miR-21, miR-196a, miR-451a and miR-1246 in six cell line-derived sEVs measured by EXTRA-CRISPR. The miRNA expression level was normalized by the input number of sEV particles for each cell line. The colour-coded miRNA level indicates the mean of two technical replicates of each assay. ND, not detected.

to afford highly specific detection of the four miRNA targets with minimal cross-reactivity between individual padlock probes and three non-targets (Fig. 5d). Overall, these results corroborate the excellent adaptability of the EXTRA-CRISPR method to sensitive and specific detection of miRNAs with competitive performance to RT-qPCR.

The one-pot EXTRA-CRISPR assays were assessed using purified EVs from human adult dermal fibroblasts (HADF) and human primary pancreatic fibroblast (HPPF) as the normal controls, PDAC cell lines (MIA-PaCa-2 and PANC-1) and xenograft cell lines derived from patients with PDAC (PC1 and PC5). sEVs were isolated from the conditioned media by ultracentrifugation[74] and characterized by nanoparticle tracking analysis (NTA) and transmission electron microscopy (TEM). The majority of isolated EVs showed relatively small sizes within a range of ~40–250 nm (Fig. 5e), which is typically observed for

ultracentrifugation isolates[75,76] and the morphological characteristics of sEVs (Fig. 5f)[75,76]. The abundance of each cell line-derived sEV was also measured by NTA to prepare standards for quantitative assessment of the one-pot miRNA assays. Using a commercial exosome antibody array, the quality of EV preparations was further verified by positive detection of several generic exosome protein markers (for example, tetraspanins, Alix, ANXA5 and TSG101) and a weak signal for GM130, a control for cellular contamination (Fig. 5g).

We conducted miRNA profiling of MIA-PaCa-2 (MIA)-derived sEVs using the established EXTRA-CRISPR and RT-qPCR assays in parallel (Methods). As depicted in Fig. 5h, the one-pot assay yields high consistency with RT-qPCR in measuring the concentration of miR-21 (97.42 fM by one-pot versus 90.13 fM by RT-qPCR) and miR-1246 (6.43 pM by one-pot versus 6.35 pM by RT-qPCR) in the samples. However, miR-196a was only detected by our one-pot assay with a determined concentration of 56.7 fM. For RT-qPCR analysis, we experienced a Ct value larger than 35 cycles for miR-196a in MIA-sEVs, which prevented precise quantification. This unexpected qPCR omission can be presumably attributed to the assumption that the poly(A)-tailing method may not be robust enough to reverse transcribe miR-196a in the intricate miRNA extract where unexpected secondary structures and hybridization may hinder RT[77]. In contrast, our one-pot assay benefits from a denaturing and annealing step in sample preparation that eliminates potential secondary structures, empowering its robustness for detecting miRNAs in complicated biological samples. The level of miR-451a in MIA sEVs appeared to be too low to be quantifiable for both methods (Fig. 5h). The abundance of the targeted sEV-miRNAs for all six cell lines were measured by the one-pot assays and summarized in Fig. 5i. Compared with HADF and HPPF control cell lines, three miRNAs (miR-21, miR-196a and miR-1246) were elevated in EVs from the PDAC-derived cell lines, while miR-451a was non-detectable in HPPF and MIA sEVs and very low (<~0.02 copies per EV) in the other four cell line-derived sEVs. Relatively high miR-196a and miR-1246 levels were observed in PDAC cell-derived sEVs, which is consistent with the previous study[67]. These findings on cell lines warrant further investigation of these sEV-miRNA markers using clinical human specimens for potential application to liquid biopsy-based diagnosis of PDAC.

We next assessed the EXTRA-CRISPR assay for measuring clinical plasma samples from cancer-free controls ($n = 15$) and patients with PDAC ($n = 20$) (Supplementary Table 4). As illustrated in Fig. 5a, the analysis workflow starts with isolating total circulating EVs from these plasma fluids (0.2 ml each) for subsequent small RNA extraction. To this end, a commercial polyethylene glycol precipitation kit was used to afford faster and more efficient EV isolation than ultracentrifugation and hence to maximize the miRNA yield[78,79]. NTA analysis revealed the notable subject-to-subject heterogeneity in EV abundance varying from 6×10^{10} to 58×10^{10} EVs per ml and in mean diameters of ~98–143 nm with the major size ranges from ~40 to 250 nm (Fig. 6a and Supplementary Fig. 19). The isolated plasma EVs were also checked with TEM, which showed the consistent vesicle sizes and the characteristic cup or round-shaped morphologies (Fig. 6b). Statistical comparison showed no significant difference between the control and patient groups in the NTA-measured EV levels ($P = 0.79$) and mean sizes ($P = 0.70$), respectively (Supplementary Fig. 19). We further assessed the EV quality with the exosome antibody array, which verified highly enriched exosomal vesicles against other cellular contaminations in these plasma EV preparations (Fig. 6c).

Next, we extracted and measured EV-miRNAs with the EXTRA-CRISPR to quantify the levels of miR-21, miR-196a, miR-451a and miR-1246 simultaneously. Although a spike-in control is usually used for normalization of miRNA extraction and quantification, this approach remains arguable because of the lack of reliable reference miRNA in EVs, variations in extraction efficiency for reference RNAs versus miRNAs in biofluids, and different stability of spike-in miRNAs in blood compared with the endogenous ones[45,80–83]. Therefore, we assessed our assay for potential clinical analysis without using known miRNA and small RNA controls, such as U6 that was found unsuitable for qPCR quantification of circulating miRNAs[84,85]. To ensure the rigor of our analysis, we first tested the repeatability of our miRNA extraction protocol based on a commercial kit using sEVs isolated from five human plasma samples. As shown in Supplementary Fig. 20, our miRNA extraction protocol confers excellent reproducibility for extraction of two different spike-in controls from EVs (0.4% coefficient of variation (CV) for UniSp2 and 0.5%CV for UniSp4). We also used constant input volume of different plasma samples and considered the variation in EV abundance among different subjects as a biological noise for disease diagnosis[82]. To mitigate batch-to-batch variation in our measurements, a synthetic copy of each miRNA marker was assayed as the positive control along with the clinical samples for data normalization. Lastly, we rigorously validate the EXTRA-CRISPR results by the standard RT-qPCR measurements of the same samples in parallel.

Figure 6d summarizes the concentrations of the four individual plasma EV-miRNA markers for each subject calculated from the calibration plots, showing their elevated expression in the PDAC cohort, in line with the previous studies[67,70,86]. It is noted that compared with the other three EV-miRNAs, miR-196a showed lower abundance in most of the tested clinical samples and less difference between the healthy and PDAC groups. Consistently, machine learning analysis of the data using the least absolute shrinkage and selection operator (Lasso) regression eliminated miR-196a and defined an EV-Sig of each subject as the weighted linear combination of miR-21, miR-451a and miR-1246 (Fig. 6d and Methods). As plotted in Fig. 6e, the EV-Sig improves the ability to differentiate the PDAC group against the healthy group ($P = 0.0012$, two-tailed Student's t-test with Welch correction), compared with the individual markers (miR-21, $P = 0.0026$; miR-196a, $P = 0.031$; miR-451a, $P = 0.0074$; and miR-1246, $P = 0.027$). The diagnostic performance of these EV-miRNAs and EV-Sig was quantitatively evaluated by receiver operating characteristic (ROC) curve analysis (Fig. 6f). Single-marker detection yielded modest area under the curve (AUC) values ranging from 0.677 (95% confidence interval (CI), 0.486–0.868) for miR-196a to 0.793 (95% CI, 0.635–0.951) for miR-451a. The EV-Sig panel combining miR-21, miR-451a and miR-1246 greatly improves the diagnostic power to an AUC of 0.853 (95% CI, 0.726–0.979).

To validate the EXTRA-CRISPR measurements, the same RNA extracts were analysed by the established RT-qPCR assays in parallel to quantify the four EV-miRNA markers (Supplementary Fig. 21). Strong correlation was observed between the two methods for detecting miR-21 and miR-451a, as indicated by the Pearson's r of −0.9439 and −0.9587, respectively (Fig. 6g,h). The correlation obtained for miR-1246 was modest (Pearson's $r = -0.7231$), which can be attributed to the ultralow levels of miR-1246 in most of the samples (Ct > 32) that leads to large variations in analysis (Fig. 6i). Consistent with the cell line results (Fig. 5h), the poly(A)-tailing RT-PCR assay was unable to detect EV-miR-196a in 40 thermal cycles for almost all the clinical samples tested, while the EXTRA-CRISPR assay detected the low-abundance EV-miR-196a in these samples. Thus, the RT-qPCR results of miR-21, miR-451a and miR-1246 were assessed by ROC analysis, yielding AUC values consistent with that of one-pot assays (Supplementary Fig. 22). The RT-qPCR signature combining three markers obtained through Lasso regression confers an AUC of 0.874 (95% CI, 0.757–0.991) for PDAC detection. This suggests that our assay confers a competitive performance with the RT-qPCR counterpart for plasma EV-based diagnostics targeting the same three-miRNA marker panel (Fig. 6j). Overall, these comparative assessments with clinical samples further support the high sensitivity, specificity and robustness of our method for miRNA analysis towards potential applications for liquid biopsy-based cancer diagnosis.

https://doi.org/10.1038/s41551-023-01033-1

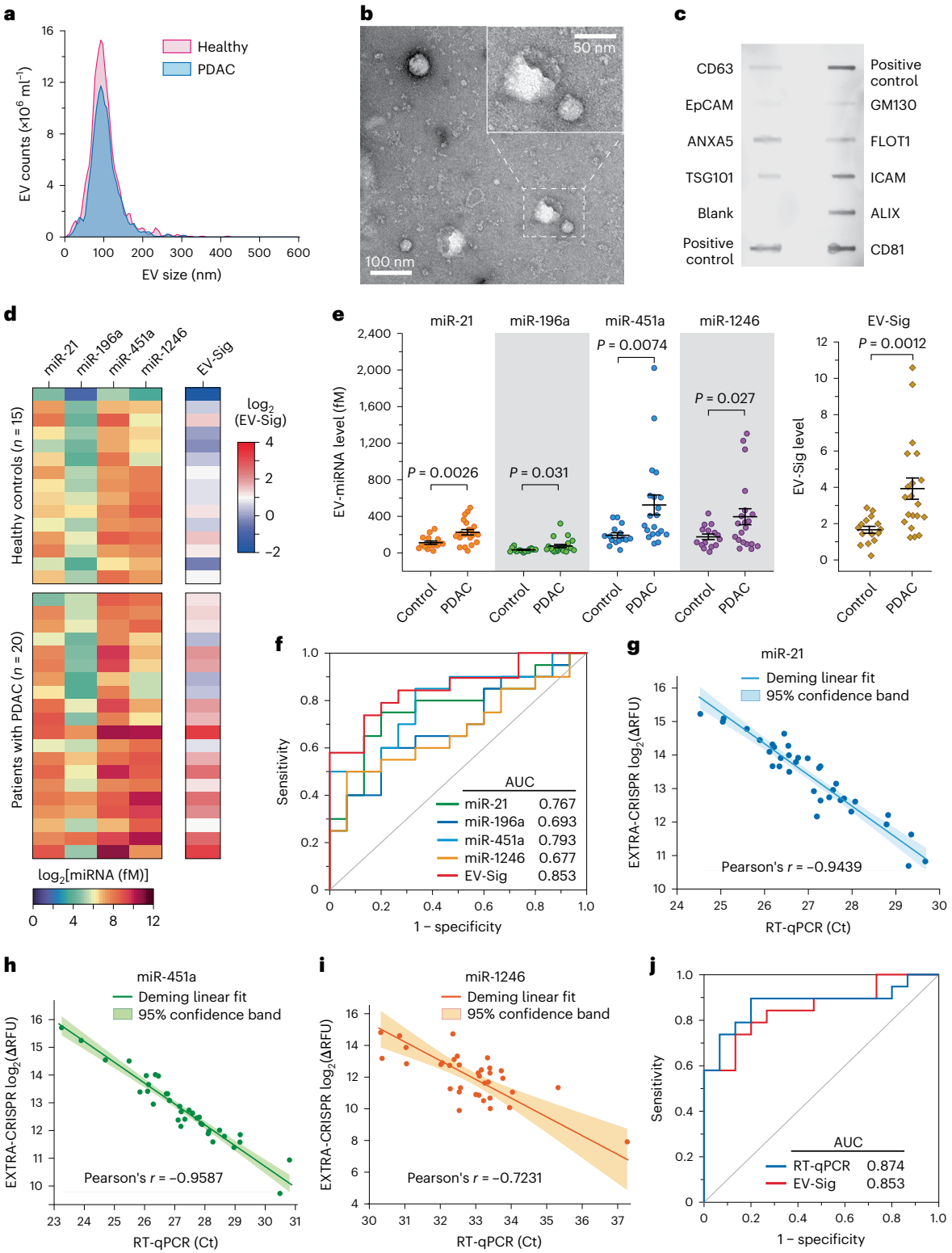


Fig. 6 | One-pot miRNA analysis for the diagnosis of pancreatic cancer. a, NTA of total EVs isolated by a precipitation kit from the plasma fluids of a healthy donor and a patient with PDAC. **b**, Representative TEM images of plasma sEVs from a patient with PDAC. **c**, Quality check of a patient-derived EV sample with the exosome antibody array; an image of the full scans is provided in Source Data. **d**, Heatmap of the expression levels of individual miRNAs in the isolated plasma EVs from the patients with PDAC ($n = 20$) and healthy donors ($n = 15$) measured by EXTRA-CRISPR. Each miRNA in each sample was tested in two technical replicates, and the background-subtracted signals were adjusted by that of the positive control. The EV-Sig was defined by the weighted linear combination of four miRNAs using Lasso regression. **e**, Scatter plots of individual sEV-miRNA markers and EV-Sig for discriminating the PDAC group from the control group. The middle line and error bar represent the mean and 1 s.e.m., respectively. *P* values were calculated by two-tailed Student's *t*-test with Welch correction. **f**, ROC curves and AUC analysis of individual sEV-miRNAs and the EV-Sig for PDAC diagnosis. **g**–**i**, Correlation between the parallel measurements by EXTRA-CRISPR and RT-qPCR for miR-21 (**g**), miR-451a (**h**) and miR-1246 (**i**). The data points represent the mean of two replicates of each measurement by each method. Linear Deming fitting of the data points was performed to generate the linear correlation curves. **j**, Comparing the EXTRA-CRISPR-based EV-Sig and the RT-qPCR tests of the four-miRNA panel for PDAC diagnosis. The RT-qPCR results of miR-21, miR-451a and miR-1246 were assessed by Lasso regression and ROC analysis. All statistical analyses were performed at 95% confidence level.

EXTRA-CRISPR assay for POC testing

The simplicity of our isothermal one-pot EXTRA-CRISPR miRNA assay makes it intrinsically adaptable to POC applications where a minimal need for instruments is desired. To test such feasibility, we attempted to build a low-cost, portable smartphone-based EXTRA-CRISPR assay system. This prototype was assembled from 3D-printed body parts, a blue light-emitting diode (LED) illuminator, a plastic filter (520 nm long-pass) and a consumer digital hotplate (coffee mug warmer) (Fig. 7a, Supplementary Fig. 23 and Supplementary Table 5). A smartphone was mounted on the device to acquire fluorescence images which were then analysed to measure the fluorescence intensity. We first assessed the POC prototype for the isothermal EXTRA-CRISPR reaction in comparison with the commercial qPCR thermocycler. In this case, the reaction tubes were simply laid on the flat hotplate surface inside the POC device which was kept at 37°C to conduct the reaction for 2 h. This simple heating method was found to preserve ~84% of the amplification efficiency obtained with the sophisticated PCR thermocycler (Supplementary Fig. 24), indicating the robustness of EXTRA-CRISPR assay that negates sophisticated heater design for precise temperature control. The smartphone-based POC device was then tested for real-time fluorescence detection of the EXTRA-CRISPR reactions. The observed detection curves were consistent with those of the RT-qPCR instrument (Fig. 7b), showing good performance of the prototype for quantitative miRNA detection. We further calibrated the POC device via targeting three miRNA markers selected above for pancreatic cancer detection, as presented in Fig. 7c–e. Compared with the EXTRA-CRISPR detection using the qPCR machine, coupling the assay with the simple low-cost device afforded slightly lower sensitivity and comparable dynamic range for miR-21 (LOD, 6.10 fM; linear range, 20–500 fM), miR-451a (9.64 fM, 10–500 fM) and miR-1246 (9.92 fM, 50–1,000 fM), respectively. Lastly, as a proof of concept for clinical applications, we assessed the POC device to detect these markers in sEVs isolated from the plasma samples of four control donors and four patients with PDAC. As seen in Fig. 7f,g, the POC device was able to detect the differential levels of three sEV-miRNA markers to discriminate the PDAC group versus the control group, which is consistent with the diagnostic results of the isothermal assays conducted on the qPCR machine (Fig. 6e).

In addition to the smartphone-based fluorescence detector, we are also interested in assessing the adaptability of our assay to instrument-free POC diagnostics. To this end, we developed an EXTRA-CRISPR test coupled with lateral flow assay (EXTRA-CRISPR-LFA) using a commercially available LFA strip for visual detection[87]. In this test, as illustrated in Fig. 7h, the ssDNA Cas12a reporter is tagged with a biotin and a carboxyfluorescein (FAM) dye molecule at each end so that it can be captured on the pre-loaded anti-FAM antibody coated gold nanoparticles when flowing through the LFA strip. The complexes formed with intact reporters will be retained on the streptavidin band via their biotin tags, producing a positive control line. If the immuno-gold particles bind with cleaved reporters, they can flow downstream to be captured by the secondary antibody deposited on the test line that specifically recognizes the anti-FAM antibody. Figure 7i presents the results for miRNA detection using the standards of three miRNAs (see Methods for details), which shows increasing intensity of the test line with the target concentration at the low levels. The test line intensity was seen to decrease at 100 pM miR-21, in consistence with the amplification suppression observed in Fig. 2. The signals for miR-451a and miR-1246 were saturated at the relatively high concentrations, which can be attributed to the limited total amount of immuno-gold nanoparticles, as indicated by the diminished intensity of corresponding control lines. Compared with the fluorescence detection modality (Fig. 7), visual LFA detection showed reduced performance for quantitative analysis, as manifested by the decreased linearity of the calibration plots, sub-100 fM LODs, and <2-log dynamic ranges (Supplementary Fig. 25). Nonetheless, it is noted that our EXTRA-CRISPR-LFA test greatly outperforms the existing LFA methods for miRNA detection with picomolar-level LODs[88].

Using the same patient samples for testing the smartphone device, we demonstrated the applicability of our EXTRA-CRISPR-LFA test for instrument-free clinical analysis of sEV-miRNAs. Among the three markers, LFA detection of sEV miR-451a yielded the highest visual signals (Fig. 7j) and the best diagnostic performance (Fig. 7k) to detect the PDAC samples, which is consistent with the results of smartphone detection (Fig. 7g). Further quantitative comparison shows a strong linear correlation between the two POC methods for detecting miR-451a (Pearson's $r = 0.949$, Fig. 7l) and miR-21 (Pearson's $r = 0.942$, Supplementary Fig. 26). Such correlation became much weaker for miR-1246 with the lowest levels detected in sEVs derived from patients with PDAC (Pearson's $r = 0.527$, Supplementary Fig. 26), due to the relatively limited sensitivity and quantitative performance of LFA. Nonetheless, these results verify the ability of our LFA assay for instrument-free semi-quantitative miRNA detection with competitive sensitivity. Overall, our proof-of-principle studies on two commonly adapted POC detection modalities suggest the potential of EXTRA-CRISPR technology as an adaptable tool for the development of new low-cost POC diagnostic tests.

Discussion

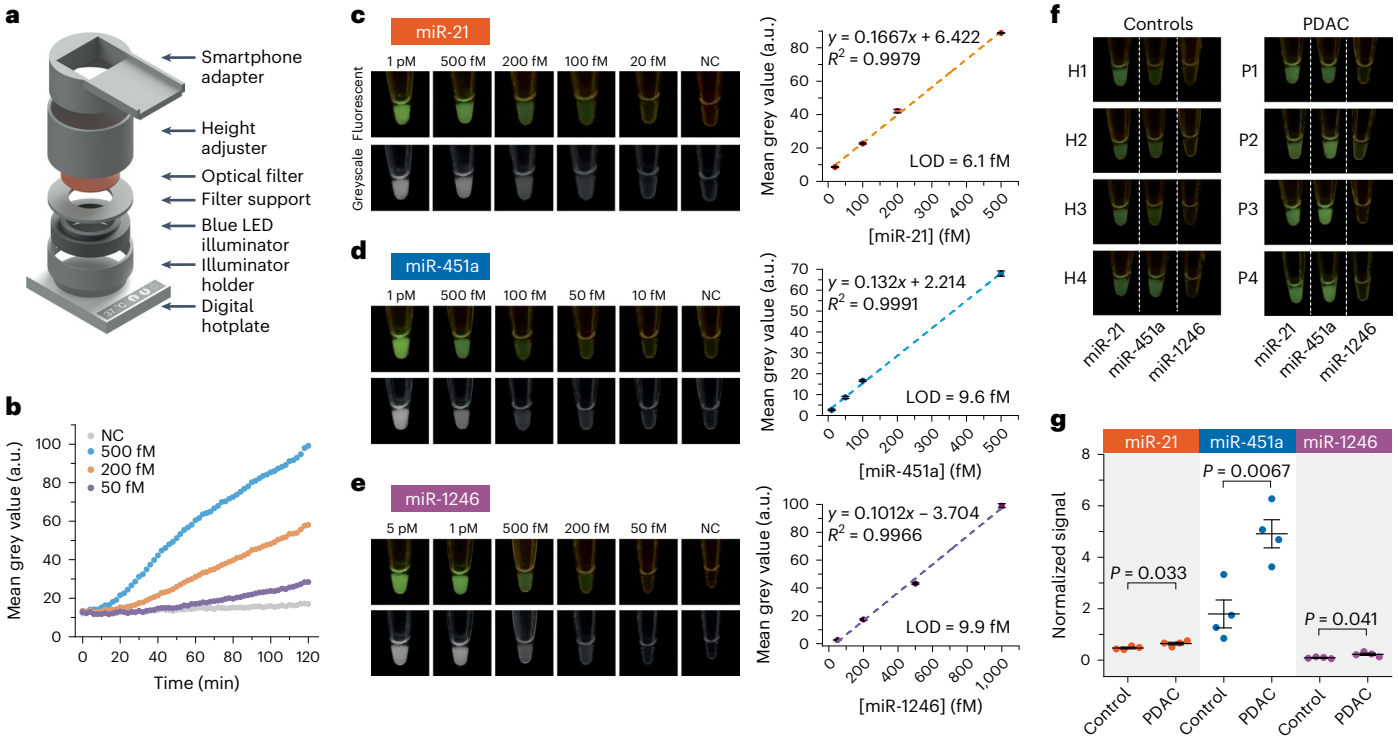
Among the many isothermal methods developed for miRNA sensing, RCA is a proven technique with advantages in simplicity, specificity and robustness. To enhance the sensitivity limited by linear amplification, several approaches have been explored to exponentiate RCA, including target-primed branched RCA using a second primer[89] and nicking-endonuclease-assisted exponential RCA[13,90]. Compared with these methods, CRISPR–Cas systems emerge as a compelling tool for miRNA detection, owing to their substantial potential to promote both detection sensitivity and specificity[30,31]. Nonetheless, as with other CRISPR-based nucleic acid tests, the prevailing strategy used in the existing methods is the tandem hyphenation of two independent reactions for miRNA pre-amplification and amplicon detection by Cas12a *trans*-cleavage (Supplementary Table 2). A challenge in combining RCA

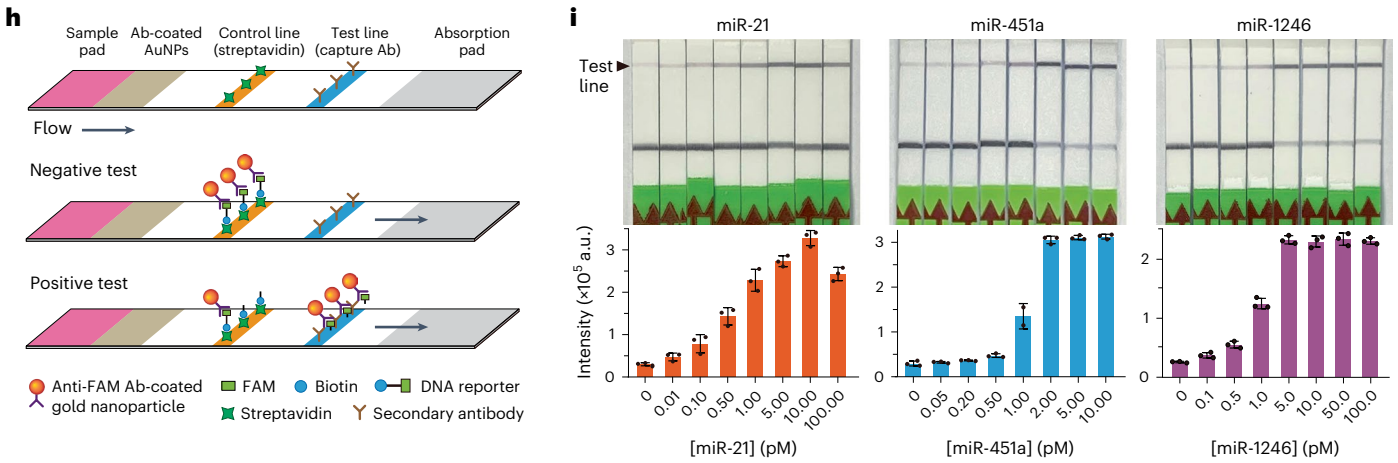
Fig. 7 | Assessment of the EXTRA-CRISPR assay for low-cost POC testing. **a**, The exploded view of a portable smartphone-based fluorescence detector assembled with 3D-printed body parts, a blue LED illuminator and a consumer digital hotplate. **b**, Real-time fluorescence detection of miR-21 using the portable EXTRA-CRISPR assay system. Images were captured every 2 min using a smartphone with an exposure time of 1 s. **c**–**e**, Representative fluorescence and corresponding greyscale images (left) acquired for calibrating the low-cost POC system for detection of miR-21 (**c**), miR-451a (**d**) and miR-1246 (**e**). The greyscale images were processed to create the background-subtracted calibration curves (right) for these three miRNAs with linear least-squares regression. Error bar, 1 s.d. ($n = 2$). **f**,**g**, Representative fluorescence images (**f**) and scatter dot plots (**g**) for detecting three miRNA markers in sEVs isolated from four control (H1–H4) and four PDAC (P1–P4) plasma samples using the POC device. To plot the scatter dot graph, the background-corrected mean grey values for each miRNA marker were normalized by that of 500 fM standard miRNA. **h**, Principle of a lateral flow assay for visual detection of the EXTRA-CRISPR product. **i**, Representative photos (top) and the bar graphs for the intensity of test lines (bottom) for the EXTRA-CRISPR-LFA detection of three miRNAs at variable concentrations. Error bar, 1 s.d. ($n = 3$). **j**,**k**, Representative photos (**j**) and scatter dot plots (**k**) for detecting three sEV-miRNA markers in the same clinical samples as in **f**. The LFA test line signals were normalized with the averaged control line intensity measured for the negative controls, respectively. In **g** and **k**, each data point represents the mean of two technical replicates. The middle line and error bar represent the population mean and 1 s.e.m., respectively. *P* values were calculated by two-tailed Student's *t*-test with Welch correction. **l**, Comparison of the results for measuring sEV miR-451a in **g** and **k** shows good correlation between the LFA and the smartphone POC device. Deming linear fitting was performed at the 95% confidence level.

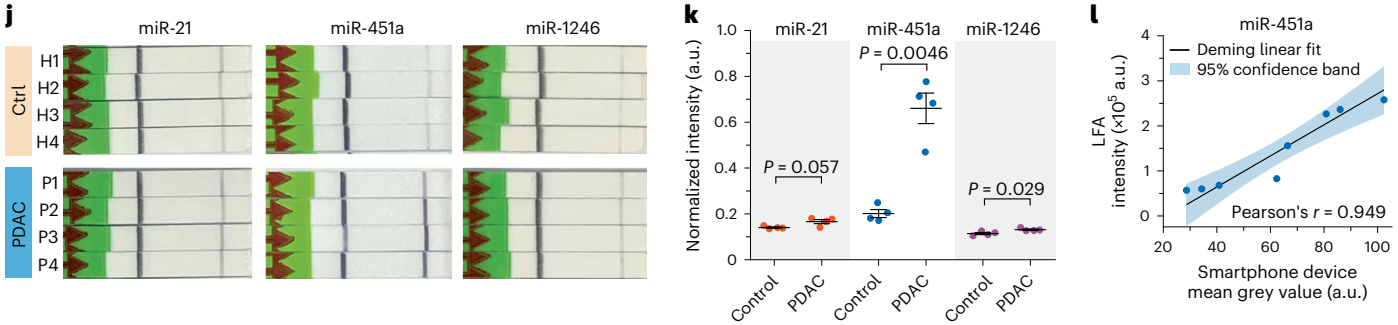
https://doi.org/10.1038/s41551-023-01033-1

(and other amplification assays) and CRISPR assays may be attributed to the double-edged effects of CRISPR–Cas12a, as revealed by our mechanistic studies (Fig. 2), where indiscriminate *trans*-cleavage of Cas12a causes the degradation of the essential ssDNA reactants (that is, the padlock probe and secondary targets) to suppress exponential amplification. To overcome this issue, we discovered a strategy that combines engineering of the CRISPR-reactive padlock probe and balancing the reaction kinetics and equilibria to promote the desired Cas12a functions in a complex tri-enzymatic reaction network (Figs. 2a and 4). This strategy allowed us to establish a one-step, one-pot isothermal assay that collaboratively couples RCA with the CRISPR–Cas12a system to enable the exponential amplification and fluorogenic detection of miRNAs. Moreover, our work suggests the feasibility of harnessing both the *cis*-cleavage and *trans*-cleavage activities of CRISPR–Cas systems for biosensing and may pave a new way for the development of CRISPR diagnostics.

High sensitivity is essential for detecting miRNA signatures of tumours in biospecimens. The concentrations of miRNA markers







in biofluids can be at the picomolar level or even lower, especially at the early disease stages[91]. Relevant to this work, the EV population is considered a major carrier of miRNAs in human biofluids, and exosomes secreted by tumour cells offer a promising route to explore disease-specific miRNA signatures[92–94]. However, it has been shown that the averaged load of a miRNA target in EVs can be as low as 10^{-5} copies per vesicle[13,95], which makes sensitive miRNA analysis essential to clinical-biomarker development. The EXTRA-CRISPR miRNA assay offers a single-digit femtomolar sensitivity and single-nucleotide specificity, which is comparable with RT-qPCR[96], while greatly simplifying and expediting the analysis workflow. The assay is also cost-effective, with the material cost estimated to be as low as US$0.60 per test at the research scale (Supplementary Table 6). Such combination of sensitive and specific analytical performance, one-pot contamination-proof operation and low cost presents our method as a substantial improvement to existing CRISPR-based miRNA assays[34,36,38,97] and a competitive alternative to other existing miRNA analysis technologies, such as droplet digital PCR[98], microarrays[99] and nanopore biosensors[82] (Supplementary Table 2).

PDAC that accounts for ~90% of all pancreatic neoplasms is a highly aggressive and lethal gastrointestinal malignancy that is projected to be the second-leading cause of cancer-related mortality by 2030, with an overall 5 year survival rate of 11% and an incidence increase rate of 0.5–1.0% per year[100–102]. Owing to its asymptomatic course, rapid progression and delayed clinical presentation, PDAC is considered a silent killer, and most patients were diagnosed at an advanced stage[103,104]. Early detection of PDAC at resectable stages has profound impact on changing the malignancy's poor survival figures[105,106]. However, no reliable screening method, either molecular or imaging-based, exists to date to allow accurate early detection of asymptomatic patients with PDAC. Serum carbohydrate antigen 19-9 (Ca19-9) detection is the most extensively adapted marker for PDAC diagnosis which was approved by the US Food and Drug Administration in 2002. Ca19-9 can help with PDAC prognosis and monitoring; however, it is not recommended as a biomarker for early detection because of its low positive predictive value (0.5–0.9%)[107]. Increasing evidence has indicated the promising potential of circulating EVs as a rapid, minimally invasive, efficient and cost-effective liquid biopsy in developing diagnostic biomarkers of PDAC[86]. Using PDAC as the disease model, we assessed the feasibility of the EXTRA-CRISPR assay for clinical analysis of miRNA markers in circulating EVs for PDAC diagnosis. Our assay shows good compatibility with two commonly used EV isolation methods. Targeting four PDAC-related markers (miR-21, miR-196a, miR-451a and miR-1246), we demonstrated highly sensitive and specific miRNA profiling of EVs derived from cell lines and clinical plasma specimens. While individual EV-miRNA tests only yielded modest diagnostic power, an EV-Sig can be defined from the four-marker panel by machine learning analysis to improve the PDAC detection with an AUC of 0.853 (Fig. 6f). This diagnostic performance is comparable with that of the serum Ca19-9 test previously reported[108], which supports the clinical potential of EV-miRNA markers for PDAC diagnosis. Rigorous validation by RT-qPCR analysis of the same samples was conducted in parallel to the one-pot assays and showed strong correlation in both analytical and diagnostic performance between the two methods, confirming the robustness of the EXTRA-CRSPR assay. It is noted that the primary goal of this proof-of-concept clinical study was to assess a bioassay rather than the biomarkers. To this end, we simply gathered the panel of four miRNAs highly associated with PDAC from literature. An improved EV-Sig, constituted with an optimal miRNA biomarker panel for PDAC diagnosis, will no doubt enhance the diagnostic power of our one-pot assay. Future work of large-scale screening and validation of circulating EV-miRNAs using the developed EXTRA-CRSPR assay could facilitate the identification of potent EV-miRNA biomarker candidates in PDAC and beyond.

Overall, featuring a combination of sensitive and specific analytical performance, easy operation, rapid reaction and low cost, EXTRA-CRISPR provides a competitive alternative to standard RT-qPCR for miRNA analysis in biological and clinical samples. The simplicity of the method would greatly facilitate future instrumentation or microfluidic miniaturization and integration to fully automate the workflow, further increase analysis throughput and reproducibility, and reduce sample consumption and turnaround time. For instance, our assay can be readily integrated with microfluidic EV isolation[109,110] to streamline the analytical pipeline and to improve the performance for clinical analysis of EV-miRNA markers. In addition to biosensing development and instrumentation, another promising application area of our one-pot EXTRA-CRISPR assay would be POC diagnostics, where cost-effective and portable devices are needed for the rapid detection of infectious pathogens in resource-limited settings. Our proof-of-concept studies using both smartphone-based and LFA-based modalities show the ability of EXTRA-CRISPR technology to afford improved analytical performance for miRNA detection when compared with existing POC methods[88]. These results support the feasibility of EXTRA-CRISPR technology to open opportunities for developing low-cost yet sensitive nucleic acid tests for broad POC applications, such as SARS-CoV-2 diagnosis[111,112]. In principle, CRISPR-enabled isothermal amplification technology could provide a versatile tool for developing new biosensors for other types of biomarker such as proteins and small molecules, using aptamers or other nucleic acids as a bridge[113,114]. We hope that the technology facilitates the development of new biosensing technologies and clinical biomarkers and open up opportunities for developing CRISPR diagnostics that address needs in biological research, clinical-lab diagnosis and POC testing.

Methods

Materials

RNA and DNA oligos were purchased from Integrated DNA Technologies. SplintR buffer, dNTP (10 mM), BSA (20 mg ml^{-1}), phi29 polymerase (10 U μl^{-1}), SplintR ligase (25 U μl^{-1}), T4 DNA ligase (400 U μl^{-1}), Cas12a (1 μM) and ATP were purchased from New England Biolabs. SYBR Green II dye, SYBR gold nucleic acid gel stain, agarose and 10× TBE buffer were purchased from Thermo Fisher Scientific. SeraMir exosome RNA amplification kit (RA806A-1), SeraMir exosome RNA column purification kit (RA808A-1) and Exo-Check exosome antibody array (EXORAY200B-4) were purchased from System Biosciences. miRCURY LNA RT kit, miRCURY LNA SYBR Green PCR kit, miRNA specific primers and the spike-in control were purchased from Qiagen. Pierce rapid gold BCA protein assay kit (A53226) was purchased from ThermoFisher Scientific. WesternBright Sirius chemiluminescent HRP substrate was purchased from Advansta.

Procedure of EXTRA-CRISPR assay

For the preparation of RNP, 2 μl of water, 0.5 μl of 2.1 buffer (New England Biolabs), 1 μl of Cas12a (1 μM) and 1.5 μl of crRNA (1 μM) was incubated together at 37 °C for 30 min. The usage of each component can be adjusted according to the experimental consumption. For a 20 μl reaction, padlock (2 μl) and miRNA (2 μl) in buffer (0.4 μl) are first denatured at 80 °C for 5 min and cooled down to room temperature in about 1 min and then added to the reaction system containing other components (15.6 μl in total, with 0.8 μl of dNTP, 0.2 μl of BSA, phi29 polymerase, SplintR ligase, RNP, reporter DNA, 1.6 μl of 10× buffer and water). After mixing, the assay was performed in a qPCR device (Bio-Rad, CFX connect real-time system) at 37 °C for a certain period, and the fluorescence intensity was monitored every 1 min. The final concentration of miRNA in the 20 μl reaction system was used to determine the analytical sensitivity.

Procedures of RCA only, two-step method and three-step method

In the RCA-only method, padlock (1 μl), miRNA (1 μl), and SplintR buffer (0.2 μl) were first denatured at 80 °C for 5 min and cooled down

gradually to room temperature before being added to the ligation system which contains 0.8 µl of SplintR buffer, 0.25 µl of SplintR ligase and 6.75 µl of water. Ligation was performed at 37 °C for 2 h and then 65 °C for 10 min. Then 2 µl of the ligation product was mixed with the 20 µl RCA reaction system which contains 2 µl of phi29 buffer, 0.4 µl of phi29, 0.2 µl of BSA, 0.8 µl of dNTP, 2 µl of 10× SYBR Green II, and 12.6 µl of water. RCA was performed at 37 °C for 2 h in the qPCR device and monitored every 1 min. The miRNA concentration in the ligation system was used to determine the analytical performance. In the two-step method, 2 µl of padlock, 2 µl of miRNA and 0.4 µl of SplintR buffer were first denatured and annealed and then transferred to the 20 µl ligation–RCA system which contains 1.6 µl of SplintR buffer, 0.8 µl of dNTP, 0.2 µl of BSA, 0.2 µl of phi29, 0.5 µl of SplintR and 12.3 µl of water. The reaction was conducted at 37 °C for 2 h and then 65 °C for 10 min. Next, 5 µl of RNP and 0.2 µl of the reporter (100 µM) were added to the system and incubated at 37 °C for 2 h in the qPCR device. The miRNA concentration in the ligation–RCA system was used to determine the analytical performance. In the three-step method, ligation and RCA step were the same with the RCA-only method; after RCA, the enzyme was inactivated at 65 °C for 10 min followed by the addition of 5 µl of RNP and 0.2 µl of the reporter (100 µM). The final step was carried out at 37 °C for 2 h in the qPCR device. The miRNA concentration in the ligation system was used to determine the analytical performance.

Agarose gel electrophoresis

The gel electrophoresis experiments were performed using 3% agarose gel in TBE buffer at 110 V for 1 h. After that, the gel was immersed into the TBE buffer containing SYBR gold dye for 30 min. The image was captured with an imager (Odyssey, LI-COR).

RT-qPCR detection of miRNAs

In this procedure, 10 µl of the RT contains 2 µl of 5× miRCURY RT reaction buffer, 1 µl of 10× miRCURY RT enzyme mix, 1 µl of miRNA and 6 µl of water. The RT system was incubated at 42 °C for 60 min and then inactivated at 95 °C for 5 min. The cDNA solution was diluted by 60× before being added to the qPCR system which contains 5 µl of 2× miRCURY SYBR green master mix, 1 µl of the PCR primer, 3 µl of cDNA template and 1 µl of water. The temperature program consisted of 95 °C for 2 min, 40 cycles of 95 °C for 10 s and 56 °C for 60 s.

Cell culture

Procedures for cell culture and the collection of EV-contained conditioned serum-free medium (SFM) were as previously described[115,116]. Briefly, immortalized PDAC cell lines (MIA-PaCa-2 and PANC-1), primary human xenograft-isolated PDAC cell lines (PC1, PC5) and human fibroblast cell lines (HADF and HPPF) were cultured in DMEM-F12 supplemented with 10% FBS and 1% antibiotic antimycotic solution. Culture medium was replaced by DMEM–SFM when ~85% confluence was reached. Conditioned SFM was collected after 48 h and stored at −80 °C until analysis.

EV isolation from cell culture medium

All the centrifugations were performed at 4 °C with the following procedure: 300 *g* for 10 min to remove cells, 2,000 *g* for 20 min to remove dead cells and cell debris, 10,000 *g* for 30 min to remove large EV particles (for example, microvesicles) and 100,000 *g* for 2 h to collect the sEV pellet. The sEVs were resuspended in 100 µl of PBS for the following NTA analysis and miRNA extraction using SeraMir exosome RNA column purification kit.

EV isolation, miRNA extraction and detection from plasma samples

Human plasma was obtained from Clinical and Translational Science Institute, University of Florida (IRB202200150). sEVs were isolated according to the protocol of the SeraMir Exosome RNA Amplification kit. First, thaw the plasma samples on ice and centrifuge at 3,000 *g* for 15 min to remove cells and cell debris, followed by centrifugation at 18,000 *g* for 30 min to remove large vesicles. All the centrifugations were performed at 4 °C. Then, 200 µl of the plasma was diluted to 250 µl with PBS before adding 60 µl of ExoQuick and incubated at 4 °C for 30 min. After incubation, the plasma was centrifuged at 16,200 *g* for 2 min to collect the pellet. EV-miRNA was purified and eluted in 30 µl of water according to the manufacturer's protocol for the following analysis. For the detection of miR-21, miR-196a and miR-1246, 2 µl of the miRNA extract was added to the one-pot assay. As the expression level of miR-451a is extremely high, the extract was diluted 10 times before being added to the one-pot assay for the precise quantitation of miR-451. The signals using one-pot assay were subtracted by the corresponding background and normalized by miRNA positive controls. miRNA concentrations were tested by RT-qPCR simultaneously; the extract was also diluted 10 times before being added to the RT system when detecting miR-451a. The cDNA solution was diluted 30× to perform the qPCR reaction.

TEM

Negative staining method is used for EV imaging. EVs were fixed in 2% paraformaldehyde for 5 min and loaded on 200 mesh copper grids. TEM was performed at the Electron Microscopy Core of University of Florida on a Hitachi 7600 TEM (Hitachi High-Technologies America) equipped with a MacroFire monochrome progressive scan CCD camera (Optronics).

NTA analysis

Particle number and size distribution of EVs isolated from medium and plasma samples were determined by NTA using a ZetaView system (Particle Metrix). Samples were diluted in PBS to an acceptable concentration, according to the manufacturer's recommendations.

Antibody arrays for the detection of exosomal biomarkers

The protein biomarkers of exosomes isolated from the PDAC cell line and the plasma of a patient with PDAC were tested using the Exo-Check exosome antibody array. Isolated EVs were resuspended in PBS, and the amount of protein in EV samples was determined by Pierce rapid gold BCA protein assay kit. About 50 µg protein was used for the antibody array according to the manufacture's protocol. Briefly, the sample was lysed by lysis buffer, and 1 µl of labelling reagent was added to the lysate followed by incubation at room temperature for 30 min with constant mixing. After removing excess labelling reagent, lysates were mixed with 5 ml of blocking buffer. The blocking buffer–labelled exosomes lysate mixture was then incubated with the antibody pre-coated membrane at 4 °C overnight on a shaker. Next day, the membrane was washed carefully with wash buffer and incubated with 5 ml of detection buffer at room temperature for 30 min. After removal of the detection buffer and washing, the membrane was developed using the WesternBright Sirius chemiluminescent HRP substrate. The image was captured using the LI-COR imager (Odyssey) with exposure time of 1 min.

Statistical analysis

Mean, standard deviation and standard error were calculated with standard formulas in Excel. To compare the patient and control groups, a two-tailed Student's *t*-test with Welch correction was performed with a significance level of $P < 0.05$. ROC analyses were performed to determine the AUC values using the OriginPro software (OriginLab Corporation). Machine learning analysis of the miRNA markers was conducted by fitting the data with the Lasso paths for regularized logistic regression[117], with the tuning parameter (l) selected by the leave-one-out cross-validation[118]. The estimated coefficients obtained for the markers by Lasso regression were used to create a weighted linear combination of the markers. Lasso regression was performed using the

JMP Pro 16 software (JMP Statistical Discovery LLC). A 95% confidence level was used for all statistical analyses.

EXTRA-CRISPR POC device

A coffee mug warmer (the digital hotplate) and LED illuminator were purchased from Amazon and Boli Optics, respectively, and other parts were designed using AutoCAD 2022 and fabricated using 3D printing (FormLabs Form 3+ SLA 3D printer). To conduct EXTRA-CRISPR reactions in the device, 15 µl of mineral oil was added to avoid evaporation, and the tubes were placed in the middle of the hotplate set to the actual temperature at 37°C to initiate the reactions. Fluorescent photos were captured using a smartphone in a darkroom, and the exposure time was 1 s. The grey value of each reaction was analysed using ImageJ 1.53k software: first, split the colour channels and keep the green channel of the image, then use the oval tool to determine the mean grey value in a certain area.

Lateral flow assay

The LFA strips were purchased from Milenia Biotec (HybriDetect, Universal Lateral Flow Assay Kit). The quenchers modified on reporters are replaced by biotin molecules (FAM-TTATT-Biotin). For the detection of miR-451a, the reporter concentration was decreased to 1 µM to avoid strong background signals; other reagents remain unchanged. The EXTRA-CRISPR reactions (20 µl) for LFA were first incubated in the PCR instrument and then mixed with 80 µl of HybriDetect assay buffer. After mixing, the HybriDetect dipstick was immersed into the solution with 5 min incubation time. The sticks were then taken out, and photos were captured using an iPhone XS. The LFA images were analysed using the ImageJ software (NIH): First, convert images into the 8-bit type and subtract background; second, set measurements to analyse the integrated density and invert the image colour; finally, use the rectangle tool to determine the intensity of the test band. To mitigate the variations from photographing, the LFA strips for the calibration and clinical studies were grouped together respectively to take the photos. Moreover, the LFA test line signals for miR-21, miR-451a and miR-1246 were normalized with the averaged control line intensity measured for the negative controls, respectively, assuming the constant amount of pre-loaded gold nanoparticles and uniform capture efficiency of the control lines across LFA strips.

Reporting summary

Further information on research design is available in the Nature Portfolio Reporting Summary linked to this article.

Data availability

The main data supporting the findings of this study are available within the paper and its Supplementary Information. The raw and analysed datasets generated during the study are available for research purposes from the corresponding author on reasonable request. Source data are provided with this paper.

References

1. Ha, M. & Kim, V. N. Regulation of microRNA biogenesis. *Nat. Rev. Mol. Cell Biol.* **15**, 509–524 (2014).
2. Di Leva, G., Garofalo, M. & Croce, C. M. MicroRNAs in cancer. *Annu. Rev. Pathol.* **9**, 287–314 (2014).
3. Inui, M., Martello, G. & Piccolo, S. MicroRNA control of signal transduction. *Nat. Rev. Mol. Cell Biol.* **11**, 252–263 (2010).
4. Lin, S. & Gregory, R. I. MicroRNA biogenesis pathways in cancer. *Nat. Rev. Cancer* **15**, 321–333 (2015).
5. Mori, M. A., Ludwig, R. G., Garcia-Martin, R., Brandao, B. B. & Kahn, C. R. Extracellular miRNAs: from biomarkers to mediators of physiology and disease. *Cell Metab.* **30**, 656–673 (2019).
6. Jet, T., Gines, G., Rondelez, Y. & Taly, V. Advances in multiplexed techniques for the detection and quantification of microRNAs. *Chem. Soc. Rev.* **50**, 4141–4161 (2021).
7. Dave, V. P. et al. MicroRNA amplification and detection technologies: opportunities and challenges for point of care diagnostics. *Lab. Invest.* **99**, 452–469 (2019).
8. Kilic, T., Erdem, A., Ozsoz, M. & Carrara, S. microRNA biosensors: opportunities and challenges among conventional and commercially available techniques. *Biosens. Bioelectron.* **99**, 525–546 (2018).
9. Ouyang, T., Liu, Z., Han, Z. & Ge, Q. MicroRNA detection specificity: recent advances and future perspective. *Anal. Chem.* **91**, 3179–3186 (2019).
10. Forero, D. A., Gonzalez-Giraldo, Y., Castro-Vega, L. J. & Barreto, G. E. qPCR-based methods for expression analysis of miRNAs. *Biotechniques* **67**, 192–199 (2019).
11. Hunt, E. A., Broyles, D., Head, T. & Deo, S. K. MicroRNA detection: current technology and research strategies. *Annu. Rev. Anal. Chem.* **8**, 217–237 (2015).
12. Deng, R., Zhang, K. & Li, J. Isothermal amplification for microRNA detection: from the test tube to the cell. *Acc. Chem. Res.* **50**, 1059–1068 (2017).
13. Cao, H., Zhou, X. & Zeng, Y. Microfluidic exponential rolling circle amplification for sensitive microRNA detection directly from biological samples. *Sens. Actuators B* **279**, 447–457 (2019).
14. Yan, H., Xu, Y., Lu, Y. & Xing, W. Reduced graphene oxide-based solid-phase extraction for the enrichment and detection of microRNA. *Anal. Chem.* **89**, 10137–10140 (2017).
15. Deng, R. et al. Toehold-initiated rolling circle amplification for visualizing individual microRNAs in situ in single cells. *Angew. Chem. Int. Ed. Engl.* **53**, 2389–2393 (2014).
16. Qian, J., Zhang, Q., Liu, M., Wang, Y. & Lu, M. A portable system for isothermal amplification and detection of exosomal microRNAs. *Biosens. Bioelectron.* **196**, 113707 (2021).
17. Jia, H. X., Li, Z. P., Liu, C. H. & Cheng, Y. Q. Ultrasensitive detection of microRNAs by exponential isothermal amplification. *Angew. Chem. Int. Ed. Engl.* **49**, 5498–5501 (2010).
18. Li, C., Li, Z., Jia, H. & Yan, J. One-step ultrasensitive detection of microRNAs with loop-mediated isothermal amplification (LAMP). *Chem. Commun.* **47**, 2595–2597 (2011).
19. Park, C. R., Park, S. J., Lee, W. G. & Hwang, B. H. Biosensors using hybridization chain reaction—design and signal amplification strategies of hybridization chain reaction. *Biotechnol. Bioprocess Eng.* **23**, 355–370 (2018).
20. Choi, H. M. et al. Programmable in situ amplification for multiplexed imaging of mRNA expression. *Nat. Biotechnol.* **28**, 1208–1212 (2010).
21. Wu, H. et al. Label-free and enzyme-free colorimetric detection of microRNA by catalyzed hairpin assembly coupled with hybridization chain reaction. *Biosens. Bioelectron.* **81**, 303–308 (2016).
22. Cheglakov, Z., Cronin, T. M., He, C. & Weizmann, Y. Live cell microRNA imaging using cascade hybridization reaction. *J. Am. Chem. Soc.* **137**, 6116–6119 (2015).
23. Aita, A. et al. Serum miRNA profiling for early PDAC diagnosis and prognosis: a retrospective study. *Biomedicines* **9**, 845 (2021).
24. Shukla, N., Yan, I. K. & Patel, T. Multiplexed detection and quantitation of extracellular vesicle RNA expression using NanoString. *Methods Mol. Biol.* **1740**, 177–185 (2018).
25. Srinivasan, S., Duval, M. X., Kaimal, V., Cuff, C. & Clarke, S. H. Assessment of methods for serum extracellular vesicle small RNA sequencing to support biomarker development. *J. Extracell. Vesicles* **8**, 1684425 (2019).
26. Guerau-de-Arellano, M., Alder, H., Ozer, H. G., Lovett-Racke, A. & Racke, M. K. miRNA profiling for biomarker discovery in multiple sclerosis: from microarray to deep sequencing. *J. Neuroimmunol.* **248**, 32–39 (2012).

27. Hong, L. Z. et al. Systematic evaluation of multiple qPCR platforms, NanoString and miRNA-Seq for microRNA biomarker discovery in human biofluids. *Sci. Rep.* **11**, 4435 (2021).
28. Kaminski, M. M., Abudayyeh, O. O., Gootenberg, J. S., Zhang, F. & Collins, J. J. CRISPR-based diagnostics. *Nat. Biomed. Eng.* **5**, 643–656 (2021).
29. Li, Y., Li, S., Wang, J. & Liu, G. CRISPR/Cas systems towards next-generation biosensing. *Trends Biotechnol.* **37**, 730–743 (2019).
30. Gootenberg, J. S. et al. Nucleic acid detection with CRISPR–Cas13a/C2c2. *Science* **356**, 438–442 (2017).
31. Chen, J. S. et al. CRISPR–Cas12a target binding unleashes indiscriminate single-stranded DNase activity. *Science* **360**, 436–439 (2018).
32. Joung, J. et al. Detection of SARS-CoV-2 with SHERLOCK one-pot testing. *N. Engl. J. Med.* **383**, 1492–1494 (2020).
33. Li, L. et al. HOLMESv2: a CRISPR–Cas12b-assisted platform for nucleic acid detection and DNA methylation quantitation. *ACS Synth. Biol.* **8**, 2228–2237 (2019).
34. Wang, G., Tian, W., Liu, X., Ren, W. & Liu, C. New CRISPR-derived microRNA sensing mechanism based on Cas12a self-powered and rolling circle transcription-unleashed real-time crRNA recruiting. *Anal. Chem.* **92**, 6702–6708 (2020).
35. Xu, L. Q. et al. Accurate MRSA identification through dual-functional aptamer and CRISPR–Cas12a assisted rolling circle amplification. *J. Microbiol. Methods* **173**, 105917 (2020).
36. Zhang, G., Zhang, L., Tong, J. T., Zhao, X. X. & Ren, J. L. CRISPR–Cas12a enhanced rolling circle amplification method for ultrasensitive miRNA detection. *Microchem. J.* **158**, 105239 (2020).
37. Zhang, M., Wang, H. H., Wang, H., Wang, F. F. & Li, Z. P. CRISPR/Cas12a-assisted ligation-initiated loop-mediated isothermal amplification (CAL-LAMP) for highly specific detection of microRNAs. *Anal. Chem.* **93**, 7942–7948 (2021).
38. Sun, H. H., He, F., Wang, T., Yin, B. C. & Ye, B. C. A Cas12a-mediated cascade amplification method for microRNA detection. *Analyst* **145**, 5547–5552 (2020).
39. Ding, X. et al. Ultrasensitive and visual detection of SARS-CoV-2 using all-in-one dual CRISPR–Cas12a assay. *Nat. Commun.* **11**, 4711 (2020).
40. Li, S. et al. A one-step, one-pot CRISPR nucleic acid detection platform (CRISPR-top): application for the diagnosis of COVID-19. *Talanta* **233**, 122591 (2021).
41. Lu, S. H. et al. Fast and sensitive detection of SARS-CoV-2 RNA using suboptimal protospacer adjacent motifs for Cas12a. *Nat. Biomed. Eng.* **6**, 286–297 (2022).
42. Bruch, R. et al. CRISPR/Cas13a-powered electrochemical microfluidic biosensor for nucleic acid amplification-free miRNA diagnostics. *Adv. Mater.* **31**, 1970365 (2019).
43. Zheng, F. et al. A highly sensitive CRISPR-empowered surface plasmon resonance sensor for diagnosis of inherited diseases with femtomolar-level real-time quantification. *Adv. Sci.* **9**, e2105231 (2022).
44. Hajian, R. et al. Detection of unamplified target genes via CRISPR–Cas9 immobilized on a graphene field-effect transistor. *Nat. Biomed. Eng.* **3**, 427–437 (2019).
45. Yan, H., Li, Y., Cheng, S. & Zeng, Y. Advances in analytical technologies for extracellular vesicles. *Anal. Chem.* **93**, 4739–4774 (2021).
46. Kalluri, R. & LeBleu, V. S. The biology, function, and biomedical applications of exosomes. *Science* **367**, eaau6977 (2020).
47. Thery, C., Zitvogel, L. & Amigorena, S. Exosomes: composition, biogenesis and function. *Nat. Rev. Immunol.* **2**, 569–579 (2002).
48. Moller, A. & Lobb, R. J. The evolving translational potential of small extracellular vesicles in cancer. *Nat. Rev. Cancer* **20**, 697–709 (2020).
49. van Niel, G., D'Angelo, G. & Raposo, G. Shedding light on the cell biology of extracellular vesicles. *Nat. Rev. Mol. Cell Biol.* **19**, 213–228 (2018).
50. Garcia-Martin, R. et al. MicroRNA sequence codes for small extracellular vesicle release and cellular retention. *Nature* **601**, 446–451 (2022).
51. Anfossi, S., Babayan, A., Pantel, K. & Calin, G. A. Clinical utility of circulating non-coding RNAs—an update. *Nat. Rev. Clin. Oncol.* **15**, 541–563 (2018).
52. Ko, J. et al. miRNA profiling of magnetic nanopore-isolated extracellular vesicles for the diagnosis of pancreatic cancer. *Cancer Res.* **78**, 3688–3697 (2018).
53. Pfeffer, S. R., Yang, C. H. & Pfeffer, L. M. The role of miR-21 in cancer. *Drug Dev. Res.* **76**, 270–277 (2015).
54. Singh, D. et al. Real-time observation of DNA target interrogation and product release by the RNA-guided endonuclease CRISPR Cpf1 (Cas12a). *Proc. Natl Acad. Sci. USA* **115**, 5444–5449 (2018).
55. Nallur, G. et al. Signal amplification by rolling circle amplification on DNA microarrays. *Nucleic Acids Res.* **29**, E118 (2001).
56. Baner, J., Nilsson, M., Mendel-Hartvig, M. & Landegren, U. Signal amplification of padlock probes by rolling circle replication. *Nucleic Acids Res.* **26**, 5073–5078 (1998).
57. Dahl, F. et al. Circle-to-circle amplification for precise and sensitive DNA analysis. *Proc. Natl Acad. Sci. USA* **101**, 4548–4553 (2004).
58. Ali, M. M. et al. Rolling circle amplification: a versatile tool for chemical biology, materials science and medicine. *Chem. Soc. Rev.* **43**, 3324–3341 (2014).
59. Lohman, G. J., Zhang, Y., Zhelkovsky, A. M., Cantor, E. J. & Evans, T. C. Jr. Efficient DNA ligation in DNA-RNA hybrid helices by Chlorella virus DNA ligase. *Nucleic Acids Res.* **42**, 1831–1844 (2014).
60. Jin, J. M., Vaud, S., Zhelkovsky, A. M., Posfai, J. & McReynolds, L. A. Sensitive and specific miRNA detection method using SplintR Ligase. *Nucleic Acids Res.* **44**, e116 (2016).
61. Wee, E. J. H. & Trau, M. Simple isothermal strategy for multiplexed, rapid, sensitive, and accurate miRNA detection. *ACS Sens.* **1**, 670–675 (2016).
62. Lagunavicius, A., Kiveryte, Z., Zimbaite-Ruskuliene, V., Radzvilavicius, T. & Janulaitis, A. Duality of polynucleotide substrates for Phi29 DNA polymerase: 3′→5′ RNase activity of the enzyme. *RNA* **14**, 503–513 (2008).
63. Bloomston, M. et al. MicroRNA expression patterns to differentiate pancreatic adenocarcinoma from normal pancreas and chronic pancreatitis. *JAMA* **297**, 1901–1908 (2007).
64. Goto, T. et al. An elevated expression of serum exosomal microRNA-191,-21,-451a of pancreatic neoplasm is considered to be efficient diagnostic marker. *BMC Cancer* **18**, 116 (2018).
65. Que, R., Ding, G., Chen, J. & Cao, L. Analysis of serum exosomal microRNAs and clinicopathologic features of patients with pancreatic adenocarcinoma. *World J. Surg. Oncol.* **11**, 219 (2013).
66. Roldo, C. et al. MicroRNA expression abnormalities in pancreatic endocrine and acinar tumors are associated with distinctive pathologic features and clinical behavior. *J. Clin. Oncol.* **24**, 4677–4684 (2006).
67. Xu, Y. F., Hannafon, B. N., Zhao, Y. D., Postier, R. G. & Ding, W. Q. Plasma exosome miR-196a and miR-1246 are potential indicators of localized pancreatic cancer. *Oncotarget* **8**, 77028–77040 (2017).
68. Szafranska, A. E. et al. MicroRNA expression alterations are linked to tumorigenesis and non-neoplastic processes in pancreatic ductal adenocarcinoma. *Oncogene* **26**, 4442–4452 (2007).
69. Zhang, Y. et al. Profiling of 95 microRNAs in pancreatic cancer cell lines and surgical specimens by real-time PCR analysis. *World J. Surg.* **33**, 698–709 (2009).

70. Vicentini, C. et al. Exosomal miRNA signatures of pancreatic lesions. *BMC Gastroenterol.* **20**, 137 (2020).
71. Takahasi, K. et al. Usefulness of exosome-encapsulated microRNA-451a as a minimally invasive biomarker for prediction of recurrence and prognosis in pancreatic ductal adenocarcinoma. *J. Hepatobiliary Pancreat. Sci.* **25**, 155–161 (2018).
72. Kawamura, S. et al. Exosome-encapsulated microRNA-4525, microRNA-451a and microRNA-21 in portal vein blood is a high-sensitive liquid biomarker for the selection of high-risk pancreatic ductal adenocarcinoma patients. *J. Hepatobiliary Pancreat. Sci.* **26**, 63–72 (2019).
73. Madhavan, B. et al. Combined evaluation of a panel of protein and miRNA serum-exosome biomarkers for pancreatic cancer diagnosis increases sensitivity and specificity. *Int. J. Cancer* **136**, 2616–2627 (2015).
74. Zhang, P., He, M. & Zeng, Y. Ultrasensitive microfluidic analysis of circulating exosomes using a nanostructured graphene oxide/polydopamine coating. *Lab Chip* **16**, 3033–3042 (2016).
75. Verel-Yilmaz, Y. et al. Extracellular vesicle-based detection of pancreatic cancer. *Front. Cell. Dev. Biol.* **9**, 697939 (2021).
76. Xu, Y. F. et al. Isolation of extra-cellular vesicles in the context of pancreatic adenocarcinomas: addition of one stringent filtration step improves recovery of specific microRNAs. *PLoS ONE* **16**, e0259563 (2021).
77. Mou, G., Wang, K., Xu, D. & Zhou, G. Evaluation of three RT-qPCR-based miRNA detection methods using seven rice miRNAs. *Biosci. Biotechnol. Biochem.* **77**, 1349–1353 (2013).
78. Andreu, Z. et al. Comparative analysis of EV isolation procedures for miRNAs detection in serum samples. *J. Extracell. Vesicles* **5**, 31655 (2016).
79. Brennan, K. et al. A comparison of methods for the isolation and separation of extracellular vesicles from protein and lipid particles in human serum. *Sci. Rep.* **10**, 1039 (2020).
80. Gouin, K. et al. A comprehensive method for identification of suitable reference genes in extracellular vesicles. *J. Extracell. Vesicles* **6**, 1347019 (2017).
81. Ragni, E. et al. miRNA reference genes in extracellular vesicles released from amniotic membrane-derived mesenchymal stromal cells. *Pharmaceutics* **12**, 347 (2020).
82. Cai, S. et al. Single-molecule amplification-free multiplexed detection of circulating microRNA cancer biomarkers from serum. *Nat. Commun.* **12**, 3515 (2021).
83. Veryaskina, Y. A. et al. Selection of reference genes for quantitative analysis of microRNA expression in three different types of cancer. *PLoS ONE* **17**, e0254304 (2022).
84. Xiang, M. et al. U6 is not a suitable endogenous control for the quantification of circulating microRNAs. *Biochem. Biophys. Res. Commun.* **454**, 210–214 (2014).
85. Lou, G. et al. Differential distribution of U6 (RNU6-1) expression in human carcinoma tissues demonstrates the requirement for caution in the internal control gene selection for microRNA quantification. *Int. J. Mol. Med.* **36**, 1400–1408 (2015).
86. Yee, N. S., Zhang, S., He, H. Z. & Zheng, S. Y. Extracellular vesicles as potential biomarkers for early detection and diagnosis of pancreatic cancer. *Biomedicines* **8**, 581 (2020).
87. Gootenberg, J. S. et al. Multiplexed and portable nucleic acid detection platform with Cas13, Cas12a, and Csm6. *Science* **360**, 439–444 (2018).
88. Wang, N. et al. Recent advances in the rapid detection of microRNA with lateral flow assays. *Biosens. Bioelectron.* **211**, 114345 (2022).
89. Cheng, Y. et al. Highly sensitive determination of microRNA using target-primed and branched rolling-circle amplification. *Angew. Chem. Int. Ed. Engl.* **121**, 3318–3322 (2009).
90. Liu, H. et al. High specific and ultrasensitive isothermal detection of microRNA by padlock probe-based exponential rolling circle amplification. *Anal. Chem.* **85**, 7941–7947 (2013).
91. Weber, J. A. et al. The microRNA spectrum in 12 body fluids. *Clin. Chem.* **56**, 1733–1741 (2010).
92. Bhome, R. et al. Exosomal microRNAs (exomiRs): small molecules with a big role in cancer. *Cancer Lett.* **420**, 228–235 (2018).
93. Salehi, M. & Sharifi, M. Exosomal miRNAs as novel cancer biomarkers: challenges and opportunities. *J. Cell. Physiol.* **233**, 6370–6380 (2018).
94. O'Brien, K., Breyne, K., Ughetto, S., Laurent, L. C. & Breakefield, X. O. RNA delivery by extracellular vesicles in mammalian cells and its applications. *Nat. Rev. Mol. Cell Biol.* **21**, 585–606 (2020).
95. Chevillet, J. R. et al. Quantitative and stoichiometric analysis of the microRNA content of exosomes. *Proc. Natl Acad. Sci. USA* **111**, 14888–14893 (2014).
96. Krepelkova, I. et al. Evaluation of miRNA detection methods for the analytical characteristics necessary for clinical utilization. *Biotechniques* **66**, 277–284 (2019).
97. Tian, W., Liu, X., Wang, G. & Liu, C. A hyperbranched transcription-activated CRISPR–Cas12a signal amplification strategy for sensitive microRNA sensing. *Chem. Commun.* **56**, 13445–13448 (2020).
98. Tian, H. et al. Precise quantitation of MicroRNA in a single cell with droplet digital PCR based on ligation reaction. *Anal. Chem.* **88**, 11384–11389 (2016).
99. Roy, S., Soh, J. H. & Ying, J. Y. A microarray platform for detecting disease-specific circulating miRNA in human serum. *Biosens. Bioelectron.* **75**, 238–246 (2016).
100. Chen, K., Wang, Q., Kornmann, M., Tian, X. & Yang, Y. The role of exosomes in pancreatic cancer from bench to clinical application: an updated review. *Front. Oncol.* **11**, 644358 (2021).
101. Park, W., Chawla, A. & O'Reilly, E. M. Pancreatic cancer: a review. *JAMA* **326**, 851–862 (2021).
102. Wong, M. C. S. et al. Global temporal patterns of pancreatic cancer and association with socioeconomic development. *Sci. Rep.* **7**, 3165 (2017).
103. Brezgyte, G., Shah, V., Jach, D. & Crnogorac-Jurcevic, T. Non-invasive biomarkers for earlier detection of pancreatic cancer-a comprehensive review. *Cancers* **13**, 2722 (2021).
104. Yang, J. S. et al. Early screening and diagnosis strategies of pancreatic cancer: a comprehensive review. *Cancer Commun.* **41**, 1257–1274 (2021).
105. Huang, L. et al. Resection of pancreatic cancer in Europe and USA: an international large-scale study highlighting large variations. *Gut* **68**, 130–139 (2019).
106. Siegel, R. L., Miller, K. D. & Jemal, A. Cancer statistics, 2018. *CA: Cancer J. Clin.* **68**, 7–30 (2018).
107. Ballehaninna, U. K. & Chamberlain, R. S. The clinical utility of serum CA 19-9 in the diagnosis, prognosis and management of pancreatic adenocarcinoma: an evidence based appraisal. *J. Gastrointest. Oncol.* **3**, 105–119 (2012).
108. Zhang, Y. et al. Tumor markers CA19-9, CA242 and CEA in the diagnosis of pancreatic cancer: a meta-analysis. *Int. J. Clin. Exp. Med.* **8**, 11683–11691 (2015).
109. Zhang, P. et al. Ultrasensitive detection of circulating exosomes with a 3D-nanopatterned microfluidic chip. *Nat. Biomed. Eng.* **3**, 438–451 (2019).
110. Zhang, P. et al. Molecular and functional extracellular vesicle analysis using nanopatterned microchips monitors tumor progression and metastasis. *Sci. Transl. Med.* **12**, eaaz2878 (2020).
111. Chandrasekaran, S. S. et al. Rapid detection of SARS-CoV-2 RNA in saliva via Cas13. *Nat. Biomed. Eng.* **6**, 944–956 (2022).

112. Zhang, T. et al. A paper-based assay for the colorimetric detection of SARS-CoV-2 variants at single-nucleotide resolution. *Nat. Biomed. Eng.* **6**, 957–967 (2022).
113. Niemeyer, C. M., Adler, M. & Wacker, R. Detecting antigens by quantitative immuno-PCR. *Nat. Protoc.* **2**, 1918–1930 (2007).
114. Li, L. et al. Nucleic acid aptamers for molecular diagnostics and therapeutics: advances and perspectives. *Angew. Chem. Int. Ed. Engl.* **60**, 2221–2231 (2021).
115. Han, S. et al. Primary outgrowth cultures are a reliable source of human pancreatic stellate cells. *Lab. Invest.* **95**, 1331–1340 (2015).
116. Han, S. et al. The proteome of pancreatic cancer-derived exosomes reveals signatures rich in key signaling pathways. *Proteomics* **19**, e1800394 (2019).
117. Tibshirani, R. Regression shrinkage and selection via the Lasso. *J. R. Stat. Soc. B* **58**, 267–288 (1996).
118. Homrighausen, D. & McDonald, D. J. Leave-one-out cross-validation is risk consistent for Lasso. *Mach. Learn.* **97**, 65–78 (2014).

Acknowledgements

We thank the University of Florida Clinical and Translational Science Institute Biorepository Facility for providing human plasma specimen. We thank Y. Li for helping with TEM analysis and G. Tushoski for helping with culturing cells and collecting conditioned medium. This study was supported in part by grants R01 CA243445, R33 CA214333, R33 CA252158A1 and R01 CA260132 from the National Institutes of Health.

Author contributions

Y.Z. conceived and supervised the project; H.Y. and Y.Z. designed the research; H.Y. performed technology development, mechanistic study, analytical characterization and clinical validation; H.Y. and Z.T. conducted the LFA experiments; H.Y. and N.H. constructed the POC device; H.Y. and Y.W. performed isolation and NTA analysis of EVs; S.H. conducted cell culture and provided culture media; S.H. helped with TEM analysis and was involved in experiment design and discussion; S.J.H. assisted in the clinical studies; H.Y. and Y.Z. analysed the data and wrote the paper. All authors edited the paper.

Competing interests

H.Y. and Y.Z. are co-inventors on a United States provisional patent application (63/313,870) based on this work. Y.Z. holds equity interest in Clara Biotech and serves on its scientific advisory board. The other authors declare no competing interests.

Additional information

Supplementary information The online version contains supplementary material available at https://doi.org/10.1038/s41551-023-01033-1.

Correspondence and requests for materials should be addressed to Yong Zeng.

Peer review information *Nature Biomedical Engineering* thanks Ruijie Deng and the other, anonymous, reviewer(s) for their contribution to the peer review of this work. Peer reviewer reports are available.

Reprints and permissions information is available at www.nature.com/reprints.

Publisher's note Springer Nature remains neutral with regard to jurisdictional claims in published maps and institutional affiliations.

Springer Nature or its licensor (e.g. a society or other partner) holds exclusive rights to this article under a publishing agreement with the author(s) or other rightsholder(s); author self-archiving of the accepted manuscript version of this article is solely governed by the terms of such publishing agreement and applicable law.

© The Author(s), under exclusive licence to Springer Nature Limited 2023

nature portfolio

Corresponding author(s): Yong Zeng

Last updated by author(s): Mar 7, 2023

Reporting Summary

Nature Portfolio wishes to improve the reproducibility of the work that we publish. This form provides structure for consistency and transparency in reporting. For further information on Nature Portfolio policies, see our Editorial Policies and the Editorial Policy Checklist.

Statistics

For all statistical analyses, confirm that the following items are present in the figure legend, table legend, main text, or Methods section.

n/a	Confirmed	
☐	☒	The exact sample size (*n*) for each experimental group/condition, given as a discrete number and unit of measurement
☐	☒	A statement on whether measurements were taken from distinct samples or whether the same sample was measured repeatedly
☐	☒	The statistical test(s) used AND whether they are one- or two-sided *Only common tests should be described solely by name; describe more complex techniques in the Methods section.*
☒	☐	A description of all covariates tested
☐	☒	A description of any assumptions or corrections, such as tests of normality and adjustment for multiple comparisons
☐	☒	A full description of the statistical parameters including central tendency (e.g. means) or other basic estimates (e.g. regression coefficient) AND variation (e.g. standard deviation) or associated estimates of uncertainty (e.g. confidence intervals)
☐	☒	For null hypothesis testing, the test statistic (e.g. *F*, *t*, *r*) with confidence intervals, effect sizes, degrees of freedom and *P* value noted *Give P values as exact values whenever suitable.*
☒	☐	For Bayesian analysis, information on the choice of priors and Markov chain Monte Carlo settings
☒	☐	For hierarchical and complex designs, identification of the appropriate level for tests and full reporting of outcomes
☐	☒	Estimates of effect sizes (e.g. Cohen's *d*, Pearson's *r*), indicating how they were calculated

Our web collection on statistics for biologists contains articles on many of the points above.

Software and code

Policy information about availability of computer code

Data collection	Real-time fluorescence data waeres collected using the Bio-Rad CFX connect real-time system and the BioTek Synergy H1 microplate reader. Gel and antibody array images were captured using Li-COR Odyssey Fc. Nanoparticle-tracking analysis was performed using the ZetaView system (Particle Metrix Inc.).
Data analysis	Mean, standard deviation, and standard error were calculated with standard formulas in Excel (Office 365). Two-tailed Student's t-test with Welch correction and ROC analyses were performed using OriginPro 2019 software. Lasso regression was performed using the JMP Pro 16 software. Fluorescence intensity in point-of-care testing and band intensity in lateral-flow assay were analysed using ImageJ (NIH).

For manuscripts utilizing custom algorithms or software that are central to the research but not yet described in published literature, software must be made available to editors and reviewers. We strongly encourage code deposition in a community repository (e.g. GitHub). See the Nature Portfolio guidelines for submitting code & software for further information.

Data

Policy information about availability of data

All manuscripts must include a data availability statement. This statement should provide the following information, where applicable:

- Accession codes, unique identifiers, or web links for publicly available datasets
- A description of any restrictions on data availability
- For clinical datasets or third party data, please ensure that the statement adheres to our policy

The main data supporting the findings of this study are available within the paper and its Supplementary Information. The raw and analysed datasets generated during the study are available for research purposes from the corresponding author on reasonable request.

Human research participants

Policy information about studies involving human research participants and Sex and Gender in Research.

Reporting on sex and gender	Human plasma samples, from males and females, were randomly pulled out from the UF CTSI Biorepository.
Population characteristics	20 PDAC plasma samples and 15 healthy control plasma samples were obtained from the UF CTSI Biorepository. Detailed population information is provided in Supplementary Table 4.
Recruitment	No participants were recruited for the study.
Ethics oversight	UF Clinical and Translational Science Institute (CTSI) Biorepository Facility under the the protocol (IRB202200150) approved by the internal Human Subjects Committee.

Note that full information on the approval of the study protocol must also be provided in the manuscript.

Field-specific reporting

Please select the one below that is the best fit for your research. If you are not sure, read the appropriate sections before making your selection.

☒ Life sciences ☐ Behavioural & social sciences ☐ Ecological, evolutionary & environmental sciences

For a reference copy of the document with all sections, see nature.com/documents/nr-reporting-summary-flat.pdf

Life sciences study design

All studies must disclose on these points even when the disclosure is negative.

Sample size	We used 20 PDAC plasma samples and 15 healthy control plasma samples. We estimated the required sample size for ROC analysis of diagnostic accuracy by comparing the area under a ROC curve (AUC) with a null hypothesis value of 0.5. The sample size takes into account the required significance level of 0.05 and a 80% power. A total sample size of 30 was sufficient for the statistical evaluation of diagnostic accuracy.
Data exclusions	No data were excluded from the analyses.
Replication	All the experiments were conducted at least in duplicate, and all attempts at replication were successful.
Randomization	Human plasma samples were randomly pulled out from the UF Clinical and Translational Science Institute (CTSI) Biorepository Facility.
Blinding	Blinding was not used because the data were quantitatively measured.

Reporting for specific materials, systems and methods

We require information from authors about some types of materials, experimental systems and methods used in many studies. Here, indicate whether each material, system or method listed is relevant to your study. If you are not sure if a list item applies to your research, read the appropriate section before selecting a response.

Materials & experimental systems

n/a	Involved in the study
☒	☐ Antibodies
☐	☒ Eukaryotic cell lines
☒	☐ Palaeontology and archaeology
☒	☐ Animals and other organisms
☒	☐ Clinical data
☒	☐ Dual use research of concern

Methods

n/a	Involved in the study
☒	☐ ChIP-seq
☒	☐ Flow cytometry
☒	☐ MRI-based neuroimaging

Eukaryotic cell lines

Policy information about cell lines and Sex and Gender in Research

Cell line source(s)	Mia PaCa-2: purchased from ATCC (CRM-CRL-1420), male Panc-1 : purchased from ATCC (CRL-1469), male HADF : purchased from ATCC (PCS-201-012) HPPF: purchased from Vitro Biopharma (SC00A5) PC1 (PPCL-46): primary cell line, female (PMID: 27102771) PC5 (PPCL-LM1): primary cell line, male (PMID: 27102771)
Authentication	All cell lines, purchased and primary, were authenticated.
Mycoplasma contamination	All cell lines tested negative for mycoplasma contamination.
Commonly misidentified lines (See ICLAC register)	No commonly misidentified cell lines were used.